Final Report

Energy Efficient Transportation Modeling

Ahmed Ghanem
Virginia Tech Transportation Institute
Phone: (540) 231-1500; Email: aghanem @vt.edu

Jinghui Wang
Virginia Tech Transportation Institute
Phone: (540) 231-1500; Email: jwang86@vt.edu

Hesham Rakha
Virginia Tech Transportation Institute
Phone: (540) 231-1505; Email: hrakha@vt.edu

Jianhe Du
Virginia Tech Transportation Institute
Phone: (540) 231-2673; Email: jdu@vtti.vt.edu

Date
May 2020

Prepared for the Urban Mobility & Equity Center, Morgan State University, CBEIS 327, 1700 E. Coldspring Lane, Baltimore, MD 21251

ACKNOWLEDGMENT

This research was funded by the Urban Mobility & Equity Center at Morgan State University and the University Transportation Center(s) Program of the U.S. Department of Transportation.

Disclaimer

The contents of this report reflect the views of the authors, who are responsible for the facts and the accuracy of the information presented herein. This document is disseminated under the sponsorship of the U.S. Department of Transportation's University Transportation Centers Program, in the interest of information exchange. The U.S. Government assumes no liability for the contents or use thereof.

1. Report No. UMEC-021	**2. Government Accession No.**	**3. Recipient's Catalog No.**
4. Title and Subtitle Energy Efficient Transportation Modeling		**5. Report Date** May 2019
		6. Performing Organization Code
7. Author(s) *Include ORCID #* Ahmed Ghanem Jinghui Wang Hesham A. Rakha (https://orcid.org/0000-0002-5845-2929) Jianhe Du (https://orcid.org/0000-0003-1321-8298		**8. Performing Organization Report No.**
9. Performing Organization Name and Address Virginia Tech Transportation Institute 3500 Transportation Research Plaza Blacksburg, VA 24061		**10. Work Unit No.**
		11. Contract or Grant No. 69A43551747123
12. Sponsoring Agency Name and Address US Department of Transportation Office of the Secretary-Research UTC Program, RDT-30 1200 New Jersey Ave., SE Washington, DC 20590		**13. Type of Report and Period Covered** Final April 2019 - May 2020
		14. Sponsoring Agency Code

15. Supplementary Notes

16. Abstract
As concerns about climate change increase, so do calls for reductions in the use of fossil fuels and a shift to more sustainable and less-polluting transportation modes. Cities and urban areas are generally more concerned about these issues because their population comprises over half of the world's population. Roadway congestion levels began to rise again during the US economy's recovery from the most recent recession. Today, congestion levels have not only returned to pre-recession levels of 2000 and earlier, but are even greater, causing more congestion-related problems. By 2014, congestion had caused travel delay to increase to 6.9 billion hours per year, up from 5.2 billion hours per year in 2000. Additionally, congestion costs increased by nearly $46 billion between 2000 and 2014, reaching $160 billion in 2014. Sustainable transportation modes, such as cycling, walking, and use of public transit and electric vehicles, can benefit the environment in many ways, including the reduction of toxic greenhouse gas emissions and noise levels. Moreover, decreasing the number of single occupant vehicles will decrease congestion levels, travel delays, and incurred travel costs. In this work, we focus on two energy-efficient modes of transportation: cycling, and rail. First, cycling is emerging as a sustainable mode of transportation with growing acceptance and popularity, which dictates a need for more planning for its support. This will depend greatly on understanding cyclists' behaviors, which requires more research into cyclist behavior modeling. Second, rail is one of the safest modes of transportation gaining popularity in the US, and will help alleviate the negative impact of greenhouse gas emissions.

17. Key Words: Cycling Modeling, Rail Simulation, Ridesharing.	**18. Distribution Statement**

19. Security Classif. (of this report) : Unclassified	**20. Security Classif. (of this page)** Unclassified	**21. No. of Pages** 42	**22. Price**

Contents

List of Figures

List of Tables

1. Introduction

As concerns about climate change increase, so do calls for reductions in the use of fossil fuels and encouraging a shift to more sustainable and less-polluting transportation modes. Cities and urban areas are more concerned about these issues because their population currently comprises over half of the world's population. By 2050, urban population is expected to increase to 66% of the world's population [1]. The vast majority of this population uses single-occupant vehicles (SOV) for daily commutes. This not only worsens the climate change problem, but also creates higher congestion levels.

Roadway congestion levels began to rise again along with the US economy's recovery from the most recent recession. Congestion levels have not only returned to the pre-recession levels of 2000 and before, but are now even greater, causing more congestion-related problems. By 2014, congestion had caused travel delay to increase to 6.9 billion hours per year, up from 5.2 billion hours per year in 2000. Additionally, congestion costs increased by nearly $46 billion between 2000 and 2014, reaching $160 billion in 2014 [2]. Sustainable transportation modes, such as cycling, walking, and use of public transit and electric vehicles, can benefit the environment in many ways, including a reduction of toxic greenhouse gas (GHG) emissions and noise levels. Moreover, decreasing the number of SOVs will decrease congestion levels, travel delays, and incurred travel costs. Encouraging and furthering the trend of using sustainable modes of transportation will require the development of tools, measures, and planning techniques similar to those used for vehicular transportation.

The abundance of advanced information and communication technologies, such as vehicle connectivity and automation, GPS, and smartphones, makes developing such tools technically feasible and cost-effective. A typical application involves directing travelers to energy-efficient modes/routes with provided route information, thus reducing trip energy consumption at the level of route planning. Multi-modal route planning generates trip itineraries with different transportation modes. For example, travelers may first drive to a metro station and make a transfer to the subway; alternatively, people may also start their trips by walking/cycling to a bus/subway station and then take public transit for the rest of their trip. Developing such a multi-modal energy-efficient routing system requires addressing key issues and developing a comprehensive modeling framework that includes modeling on-road vehicles, metro rail, pedestrians, and bikes.

This work has two main contributions to the transportation field:

1. Chapter 2 describes the development of a dynamics-based cycling acceleration model that captures cyclist aggressiveness.

2. Chapter 3 relates the development of a microscopic rail transit simulator (RailSIM) for use in a multi-modal agent-based modeling system.

2. Modeling Instantaneous Cyclist Acceleration and Deceleration Behavior

Cycling is emerging as a sustainable mode of transportation with growing acceptance and popularity. As concerns about climate change increase, cycling has arisen as an alternative to more polluting transportation modes. Moreover, cycling is not only beneficial to the environment, but can also benefit human health by incorporating physical activity into a person's daily routine.

Bikes can provide an excellent solution for short-distance transfers. One such transfer option between public and private transportation is a bike sharing system (BSS) [3]. In recent years, BSSs have been introduced in many major US cities, including New York, NY; Chicago, IL; Washington, DC; Minneapolis, MN; Boston, MA; San Francisco, CA; and San Jose, CA. The number of BSSs has grown rapidly since 2010. In 2017, the US had 119 cities with a BSS, for a total of 4,789 stations nationwide.

Cycling can also serve as a solution to travel delays incurred due to increasing congestion levels. Following the recovery of the US economy after the 2000 recession, congestion has continued to grow. By 2014, traffic delays due to congestion had increased by 30% to reach 6.9 billion hours per year compared to 5.2 billion hours per year in 2000. This cost the US economy about $160 billion between 2000 and 2014 [2]. Mitigating increasing congestion levels and travel delays is thus one of the main benefits of expanding the role of cycling in the transportation network.

The growing popularity of cycling has dictated a need for more planning to support it as a trending transportation mode. Tools, measures, and planning techniques similar to those used for other transportation modes need to be developed for cycling. The development of such tools depends greatly on understanding cyclists' behaviors, which requires more research into bicycle traffic.

In this chapter, we used cycling GPS data collected from 10 cyclists (3 females and 7 males) to develop a dynamics-based cycling acceleration model that captures cyclist aggressiveness. We augmented the model by calibrating the maximum power for average cyclists. We also developed a model that captures cyclist deceleration behavior. The results show that the acceleration model can estimate the cyclist's pedaling input with a root-mean-square error (RMSE) of less than 21% in most cases. The results also show that the deceleration model can estimate cycling deceleration with an RMSE of 12%.

This chapter mainly focuses on modeling cycling acceleration/deceleration behaviors. The remainder of this chapter is organized as follows. Related work is discussed in Section 2.1. In Section 2.2, we describe how the dataset was collected and prepared for cycling behavior modeling. The acceleration and deceleration models are discussed in Sections 2.3 and 2.4, respectively. Section 2.5 concludes the chapter and outlines future work.

2.1. Related Work

Microscopic simulation frameworks have been used extensively to assess and evaluate traffic planning tools before they are implemented in the real world. Many scientific and commercial vehicular simulation frameworks have been developed, such as INTEGRATION [4], VISSIM [5], and SUMO [6]. The accuracy and reliability of these frameworks depends mainly on understanding drivers' behaviors and their interactions with other drivers and with other modes of transportation.

Non-vehicular transportation modes such as cycling have generally not received the same level of

interest as vehicular modes. This has resulted in a gap in the literature between research studies addressing vehicular and non-vehicular traffic. One reason for the disparity is the lack of cycling field and naturalistic datasets on cyclist behaviors. The current availability of accurate sensors, including GPSs, magnetometers, and gyroscopes, allows high quality data to be collected easily.

To address this gap, many of the widely used traffic simulation tools, such as VISSIM and SUMO, have been extended to model bicycle traffic. Moreover, mixed traffic models that model both vehicles and bicycles side by side have been proposed, such as the approach proposed by Oketch [7]. In addition, researchers have greatly benefited from the huge body of research on vehicular traffic and driver behavior, adopting driver acceleration models to model cyclist behaviors. Yet, despite their similarities, driver and cyclist behaviors could differ greatly due to dynamic cyclist characteristics, such as speed, acceleration and deceleration behaviors, and physical characteristics, such as gender, size, age, and capability [8]. Generally, acceleration models are considered the core part of any simulation framework.

Acceleration models can be divided into two main categories: kinematics- models and dynamics-based models. Kinematics-based models mimic, to some extent, the car-following behavior of vehicles. Such models describe the motion of vehicles independent of the causes of motion. They study vehicle position, velocity, and acceleration without consideration of vehicle mass, the forces acting upon the vehicle, or driving patterns. For example, Ma et al. [9] adopted a kinematics-based model introduced by Akçelick et al. [10]. This model expresses acceleration as a polynomial function of speed as shown in equation (1). The model follows an intuitive U-shaped acceleration curve. It also dictates zero acceleration at the beginning and the end of acceleration process. However, the model, like any other kinematics-based model, does not describe the cause of the motion.

$$y = \chi^n(1 - \chi^m)^2 \quad (1)$$

Dynamics-based models, on the other hand, study the forces acting upon the vehicle, including tractive and resistive forces. Dynamics-based models usually relate vehicle acceleration to vehicle maximum acceleration, which does not allow them to account for driver behavior. To mitigate this drawback, Fadhloun et al. [11] proposed a model that accounts for driver aggressiveness and personal characteristics. The model makes use of the well-known fact that the power delivered by the engine cannot be assumed to be equal to the maximum engine power, but rather depends on the percentage of the throttle opening. To the best of our knowledge, no one has adopted a dynamics-based model applicable to cyclist behavior. In this work, we used Fadhloun et al.'s model as a foundation for a cyclist acceleration behavior model.

Driving a vehicle with an engine that can deliver constant power is different from cycling, where the cyclist is considered as the engine delivering variable power, which depends on human factors (gender and age) and environmental factors (road grade, elevation, and weather conditions). Due to this difference, we proposed a model to calibrate maximum power for a cyclist. The proposed cycling acceleration model captures the different personal characteristics in cyclist behaviors.

In summary, the existing body of literature lacks studies addressing cycling behaviors. To address this gap, we developed a dynamics-based cycling acceleration model that captures cyclist aggressiveness. We augmented the model by calibrating cyclist maximum power for average cyclists. We also developed a model that explains cyclist deceleration behavior. The main contribution of this chapter is

modeling cyclist aggressiveness and personal characteristics that could be essential to building a high-fidelity microscopic cycling simulation framework.

2.2. Data Collection and Processing

In this study, we benefited from GPS data that were collected using a smartphone application for a transportation mode recognition study [12]. To collect the data, 10 employees (3 females and 7 males) at the Virginia Tech Transportation Institute were asked to carry a Galaxy Nexus or a Nexus 4 smartphone, with the application installed, on their trips. Participants were asked to select the travel mode they intended to use before starting a trip, and they were able to use buttons in the application to start and stop data logging. To make sure the data collection process was as natural as possible, participants were not asked to carry the smartphone in any particular place, but rather it was left to them to decide on a location, such as in a pocket, in their palm, in a backpack, etc. Data collection was conducted in 2015 on different workdays (Monday through Friday) during working hours (8 a.m. to 6 p.m.) on different road types with different speed limits (15, 25, and 35 mph) in Blacksburg, Virginia. Each participant was asked to record data for about 30 minutes, either in one or more trips.

2.2.1. Data Processing

We pre-processed the data, and if there was a data gap of 2.5 minutes or more, the data were considered to belong to two different trips. By the end of the data pre-processing phase, we had a total 22 of bicycle trips. The smartphone application recorded time stamp, position coordinates (longitude and latitude), and speed. The road network for the Blacksburg area was constructed using ArcGIS. Using position coordinates, each trip was snapped to a set of links. Each link was considered as a linear segment between a start node and an end node, respectively. To account for link grades, elevation information was needed. We used the Bing Elevation API to get the elevation of the network nodes, which was available to a resolution of 4.78 m. To calculate the average link grade, we divided the difference between end and start node elevations by the link length. Despite the data being recorded every second, there was missing data for short periods of less than 5 seconds. Therefore, cubic spline interpolation was used to estimate the missing data.

Since GPS data do not include acceleration/deceleration information, it has to be estimated from other measurements. Since the acceleration is the rate of change in speed, it can be calculated using the forward difference method. Given the time series of measurements of speed for a participant: $v(1)$, $v(2), \ldots, v(n)$, the acceleration is calculated as

$$a(t) = \frac{v(t+1) - v(t)}{\Delta t},$$

where $a(t)$ is the acceleration rate at time t seconds and $v(t)$, $v(t+1)$ is the velocity at times t and $t+1$ seconds, respectively. Particularly, $a(n)$ is set to zero by default.

2.2.2. Power Mathematical Model

Development of mathematical models that describe the relationship between pedaling power and speed during road cycling began more than four decades ago. These models were based on a set of human and environmental parameters. It was not until 1998 that Martin et al. [13] showed that road power can be predicted accurately by a mathematical model. They recorded power during actual cycling

and compared it to the power estimated by their model, finding that the model accounted for 97% of the variation in cycling power.

Martin et al. used fundamental engineering and physical principles to model the power required to propel a bicycle and cyclist [13]. The model is based on the equilibrium of resistance power and pedaling power P_{ped} provided by a cyclist. The resistance power is the sum of potential energy power P_{pot}, aerodynamic drag P_{air}, frictional losses in the wheel bearings P_{bear}, rolling friction P_{roll}, and gain in kinetic energy P_{kin} as

$$P_{pot} + P_{air} + P_{bear} + P_{roll} + P_{kin} = \eta P_{ped},$$

where h _ 1 is the drive-chain frictional loss.

Dahmen et al. [14] compared the contributions of the resistance powers. They found that the contributions of the bearing friction P_{bear} and kinetic energy P_{kin} components were negligible. This results in three resistance power components. It should be noted that the contributions of the aerodynamic drag P_{air} and rolling friction P_{roll} components are smaller compared to the contribution of potential energy P_{pot}.

In this chapter, we used the three components model to calculate the pedaling power assuming very low frictional loss, i.e., $\eta \approx 1$ as shown in equation (2).

$$P_{pot} + P_{air} + P_{roll} = P_{ped} \tag{2}$$

In this sense, each of the resistive power components accounts for a resistive force: R_{pot}, R_{air} and R_{roll}. The potential energy force R_{pot} accounts for the amount of work done against, or by, gravity. It is related to the total mass of the bicycle and cyclist m_T as shown in equation (3.1). The air exerts a force from aerodynamic drag R_{air} against a cyclist in motion. It depends on the frontal area of the bicycle and cyclist A, the air density ρ, and the cyclist's speed, as shown in equation (3.2). The air density decreases with an increase in elevation. Since there was only a small variation in the elevation of the trips in our dataset, we used a constant air density of sea level. The rolling force R_{roll}, shown in equation (3.3), depends mainly on the road surface. The bumpier the road, the more friction a cyclist will experience and vice versa. Table 1 lists the parameters used in the model.

$$R_{pot} = m_T \; g \; sin(arctan(G)) \tag{3.1}$$

$$R_{air} = \frac{1}{2} \rho \; C_d \; A \; v^2 \tag{3.2}$$

$$R_{roll} = m_T \; g \; C_{rr} \; cos(arctan(G)) \tag{3.3}$$

The previous model applies to a constant cycling speed. However, if the cyclist rides with an acceleration a, then the pedaling power can be calculated, as shown in equation (4).

$$P_{ped} = \left[\left(P_{pot} + P_{air} + P_{roll} \right) + m \; a \right] v \tag{4}$$

Table 1. Power Model Parameters

Parameter	Value	Unit	Source
Gravitational acceleration (g)	9.81	m/s^2	literature
Road grade (G)	variable	dimensionless	-
Air density (ρ)	1.226	kg/m^3	literature
Frontal area (A)	0.5	m^2	literature
Drag coefficient (C_d)	0.5	dimensionless	literature
Rolling coefficient (C_{rr})	0.004	dimensionless	literature

2.2.3. Cycling Profiles

Generally, a cyclist can only have three different cycling behaviors: acceleration behavior, cruising behavior, and deceleration behavior. The cycling behavior depends on several human factors (gender, age) and environmental factors (road grade, elevation, and weather conditions). Depending on the rate of change in cycling speed (acceleration rate), cycling behavior can be identified. More specifically, if a cyclist's current speed is less than the cyclist's target speed, then speed needs to be increased (positive acceleration rate), and vice versa if current speed is greater than target speed. Cycling behavior can be summarized by equation (5).

$$a(t) = \begin{cases} a^{acc}(t), & if\ v(t) < v_f \\ a^{dec}(t), & if\ v(t) > v_f \\ 0, & otherwise \end{cases} \quad (5)$$

Profiling cycling trips to extract cycling behaviors was critical to our study. We started by identifying continuous acceleration/deceleration behaviors, referred to as profiles. In addition, we used a certain set of criteria, similar to those used in [9], to select significant profiles that could be beneficial to our study. The selection criteria were based on the overall examination and inspection of the cycling trips dataset as listed below:

- The acceleration profile should be longer than 5 s.
- The acceleration profile initial speed should be between 0 and 0.5 m/s.
- The acceleration profile final speed should be greater than 1.5 m/s.
- The deceleration profile should be longer than 10 s.

2.3. Acceleration Model Development

In comparison to research efforts to model driver behavior and simulate vehicle traffic, cyclist behavior and bicycle traffic have received little attention in the literature. Attempts have been made to extend vehicle traffic simulators to include bicycles. Additionally, there are a few studies that work on understanding cyclist behavior toward building high-fidelity models for bicycle movements. Ma et al. [9] used GPS data to build a cyclist acceleration (deceleration) model to be implemented in bicycle traffic simulators. They adopted a kinematics-based polynomial model

introduced by Akçelik et al. [10] that was used to model driver acceleration. As discussed before, these models study the properties of motion, such as position, velocity, and acceleration, without consideration of the causes of the motion. Put another way, these models do not study vehicle mass, forces acting upon the vehicle, or driving patterns. Dynamics-based models, on the other hand, take forces into account.

2.3.1. Acceleration Model

In this work, we adopted a dynamics-based model first proposed by Fadhloun et al. [11]. In addition to addressing the drawbacks of kinematics-based models, it also accounts for different driving behaviors. In contrast to the previous dynamics-based model, this model does not relate acceleration to maximum acceleration. Hence, driver aggressiveness and personal characteristics affect the shape of the acceleration profile. The model makes use of the well-known fact that the power delivered by the engine cannot be assumed to be equal to the maximum engine power, but rather depends on the percentage of open throttle. This means that the shape of acceleration depends on the driver's aggressiveness in hitting the gas pedal. The model proposed a hyperbolic function that requires the calibration of three parameters for each driver as shown in equation (6).

$$t(x) = \frac{x}{\frac{x}{t_\alpha} + \frac{t_1}{2\alpha - 1} + \frac{(\alpha - x)^2}{1 - x}} \tag{6}$$

$$0.5 < \alpha \leq 1 \tag{6.1}$$

$$0.5 \leq t_\alpha < 1 \tag{6.2}$$

$$t_1 = \frac{2\alpha - 1}{\alpha t_\alpha} \tag{6.3}$$

Here $x = \frac{v}{v_f}$ is the ratio of current speed to the final (target) speed. Based on the physical phenomenon of acceleration, the authors suggested the constraints in equations (6.1) to (6.3).

2.3.2. Acceleration Model Calibration

Analogous to the latter model [11], we argue that cycling behavior can be modeled in a similar fashion. Instead of having an engine that delivers a certain power depending on the throttle opening, the cyclist is considered the engine delivering power depending on the pedaling input. More precisely, we can look at the pedaling input as a reduction factor of the maximum power a cyclist delivers to adjust the pedaling power. The pedaling power can be expressed as shown in (7).

$$P_{ped} = P_{max} \times t(x) \tag{7}$$

where P_{max} is the maximum power that can be delivered by a certain cyclist and $t(x)$ represents the pedaling input.

We started by investigating the acceleration profiles extracted from the dataset. For each profile, we used the final speed as the profile target speed. This way we can express cyclist pedaling power as a function of x. We found that different power levels are delivered depending on where and when the

acceleration profile took place on the trip. In other words, the pedaling power depends on the road grade and how tired the cyclist is. In order to develop a model that is independent of these parameters, we aggregated the acceleration profiles of each cyclist. For each cyclist, we normalized the pedaling power by the cyclist's maximum pedaling power. We calibrated the pedaling input parameters for each cyclist individually by minimizing the RMSE, calculated as follows.

$$RMSE = \sqrt{\frac{\sum_{i=1}^{n}(\hat{x}_i - x_i)^2}{n}}$$

Table 2 shows the calibrated model parameters for each cyclist alongside each associated RMSE value. It should be noted that each cyclist had between one and four acceleration profiles, except cyclist 4, who did not have any acceleration profiles to be considered. Most of the time, RMSE was less than 0.21, except for cyclists 3 and 9. For these cyclists, there was a lot of high frequency change in the pedaling power. The pedal input functions for all cyclists are shown in Figure 1.

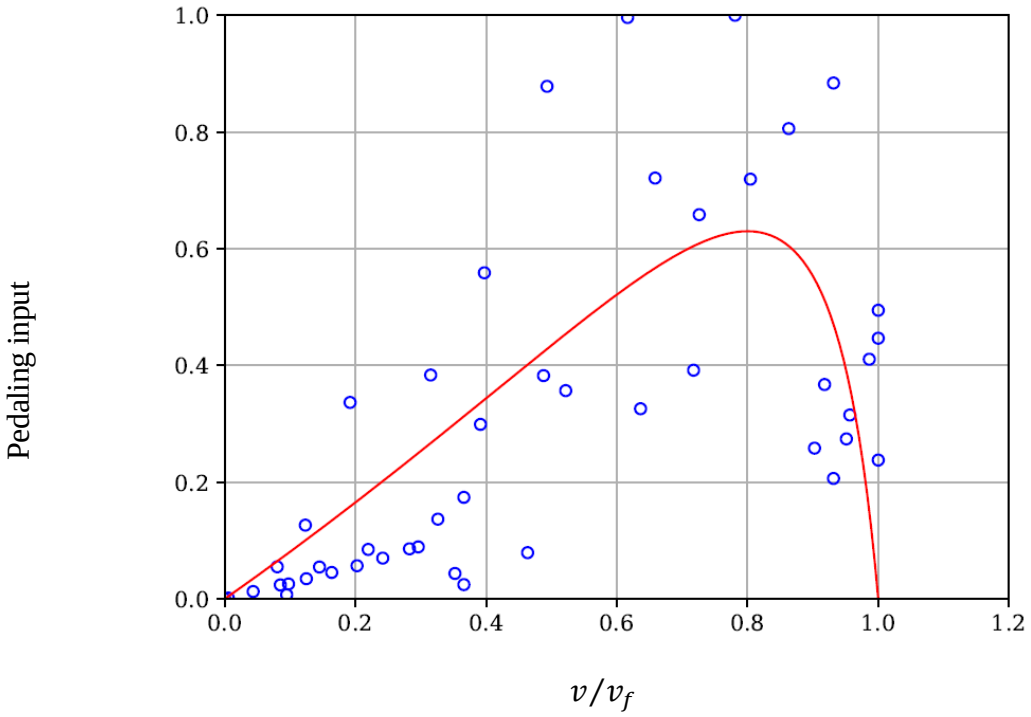

a) Cyclist 1

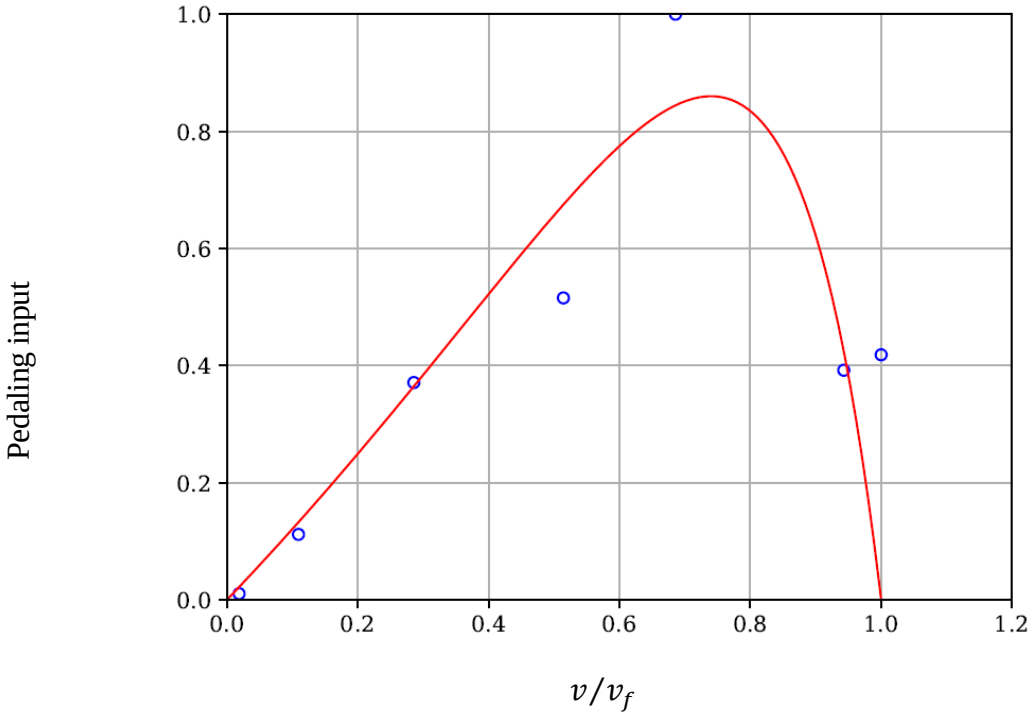

b) Cyclist 2

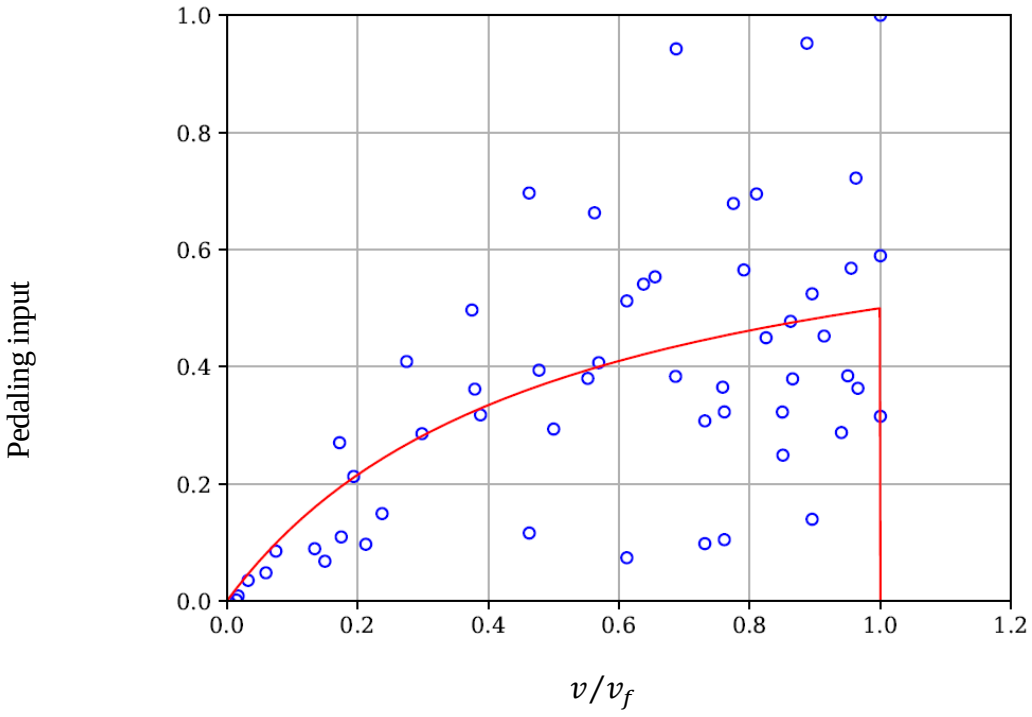

c) Cyclist 3

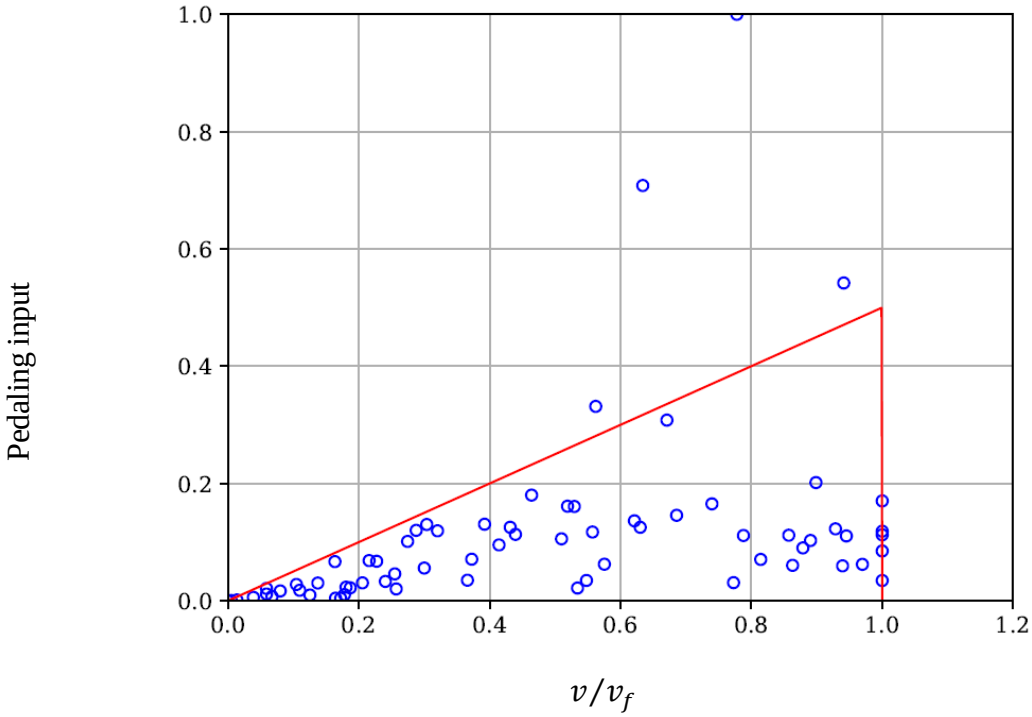

d) Cyclist 5

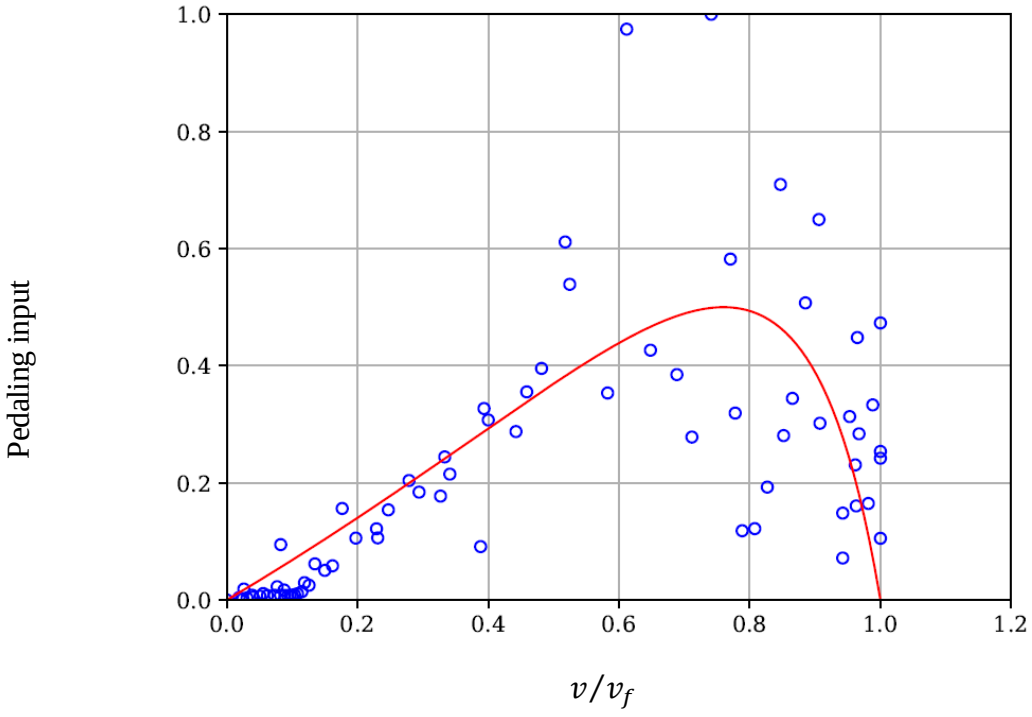

e) Cyclist 6

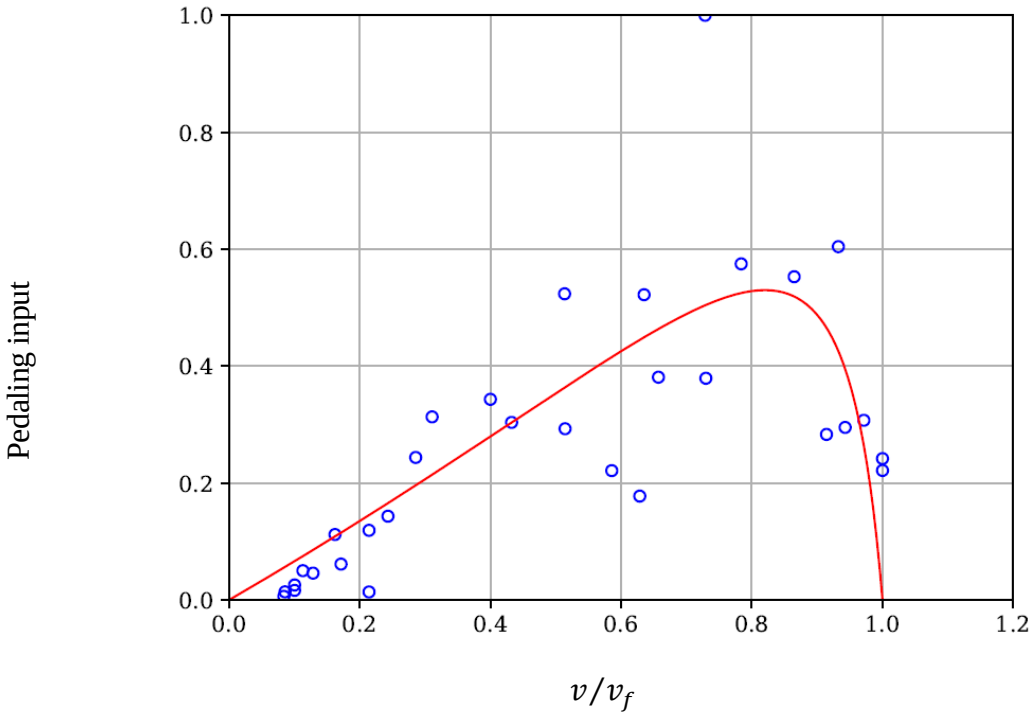

f) Cyclist 7

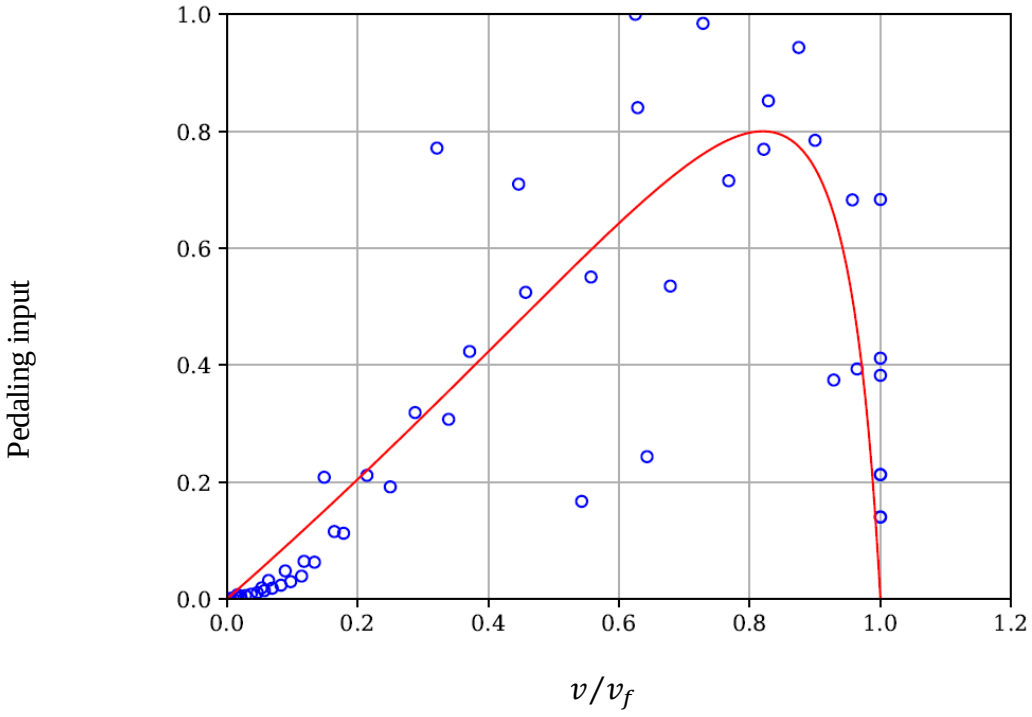

g) Cyclist 8

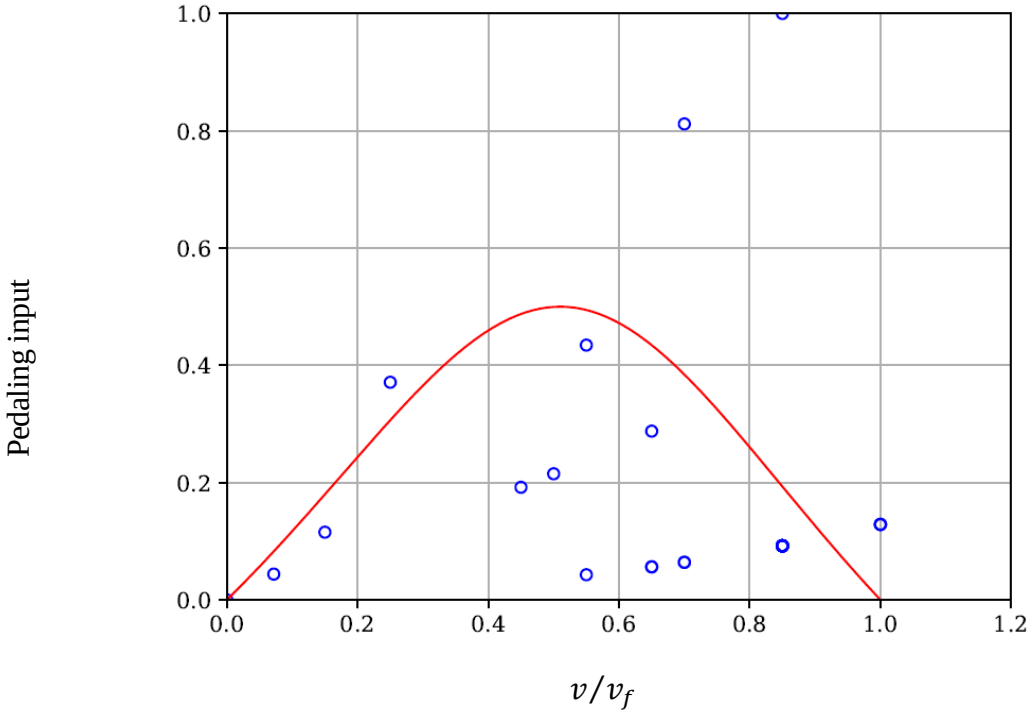

h) Cyclist 9

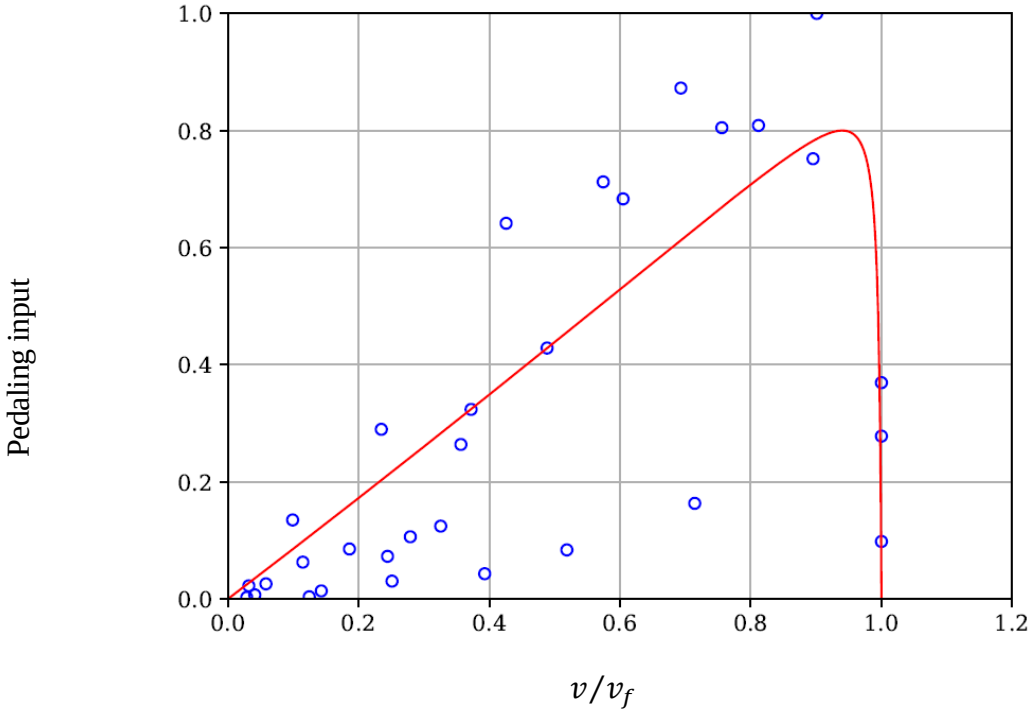

i) Cyclist 10

Figure 1. Pedaling input as a Function of Speed for Different Cyclists

Table 2. Acceleration Model Parameters

Cyclist	α	t_α	t_1	RMSE
1	0.80	0.63	1.19	0.2170
2	0.74	0.86	0.75	0.1798
3	1.00	0.50	0.66	0.2402
5	1.00	0.50	2.00	0.1925
6	0.76	0.50	1.36	0.1596
7	0.82	0.53	1.47	0.1447
8	0.82	0.80	0.97	0.1921
9	0.51	0.50	0.07	0.2519
10	0.94	0.80	1.17	0.1875

The point (α, tα) gives an idea of how aggressive a cyclist is; i.e., how a cyclist accelerates and for how long. Moreover, t1 specifies the curvature of the pedaling input function to the left of point (α, tα). This hyperbolic function realizes the fact that the acceleration varies based on the current speed and how close it is to the target speed. In the meantime, this hyperbolic function satisfies the initial condition of zero acceleration at rest; i.e., a = 0 when v = 0. Figure 1 shows that cyclist 8 accelerates more aggressively than cyclists 6 and 7. More specifically, cyclist 8 keeps increasing pedaling power to reach the target speed faster. It also shows that cyclists 7 and 8 accelerate until they reach 82% of their target speeds, but cyclist 6 accelerates to only 76% of the target speed.

Thus far, the proposed model dictates that the pedaling input is zero when the cyclist reaches the target speed. This means that the cyclist is decelerating and eventually will come to a stop. However, to maintain the target speed, the cyclist should cruise with zero acceleration: a = 0. Pedaling input can be calculated by solving (6) under the former condition. The acceleration model becomes the following equation (8).

$$t(x) = \begin{cases} \dfrac{x}{\dfrac{x}{t_\alpha} + \dfrac{t_1}{2\alpha - 1} + \dfrac{(\alpha - x)^2}{1 - x}}, & if\ v < v_f \\ \dfrac{\left(R_{pot} + R_{air} + R_{roll}\right) v}{P_{max}}, & if\ v = v_f \end{cases} \tag{8}$$

2.3.3. Maximum Power Calibration

The next step toward a complete cycling acceleration model would be to find a way to estimate a cyclist's maximum power. In contrast to constant vehicle power, a cyclist can deliver variable power depending on the exercise duration (T). Poole et al. [15] showed that in whole-body exercise such as cycling, the output power decreases hyperbolically with increasing exercise duration. They proved that this relationship can be transformed to a linear relationship between power and the reciprocal of the exercise duration. The power can be calculated as

$$P = b + (a/T),$$

where *b* is the critical power (CP; i.e., the output power that could be sustained for a long time without

fatigue). The concept of CP has been applied to other modes of exercise such as running [16] and swimming [17]. CP defines the cyclist's output power threshold, above which blood lactate starts to accumulate and stored energy sources deplete until exhaustion.

We decided to use CP as an estimate for the maximum cycling power because average cyclists tend to output power without being totally exhausted by the end of their trips. To calibrate CP for different cyclists, we used the maximal mean value method used in the cycleRtools R package. The method works by building a linear $P-1/T$ relationship. First, it specifies a duration T and calculates a moving average of the power exerted in windows of T seconds. A cyclist's maximum power over the T duration is the maximum of the moving averages of windows of T seconds. The CP is the intercept of the $P-1/T$ relationship.

When we used the maximal mean value method on our dataset, we found that the CPs were too low. This is because we never asked the cyclists to perform at maximal effort as athletes do in competitions. Consequently, we decided to use the 90th percentile instead of using the average. Evidently, this assumption did not violate the $P-1/T$ linear relationship, as shown in Figure 2b. Figure 2a shows the hyperbolic relationship between output power and time to exhaustion for cyclist 8.

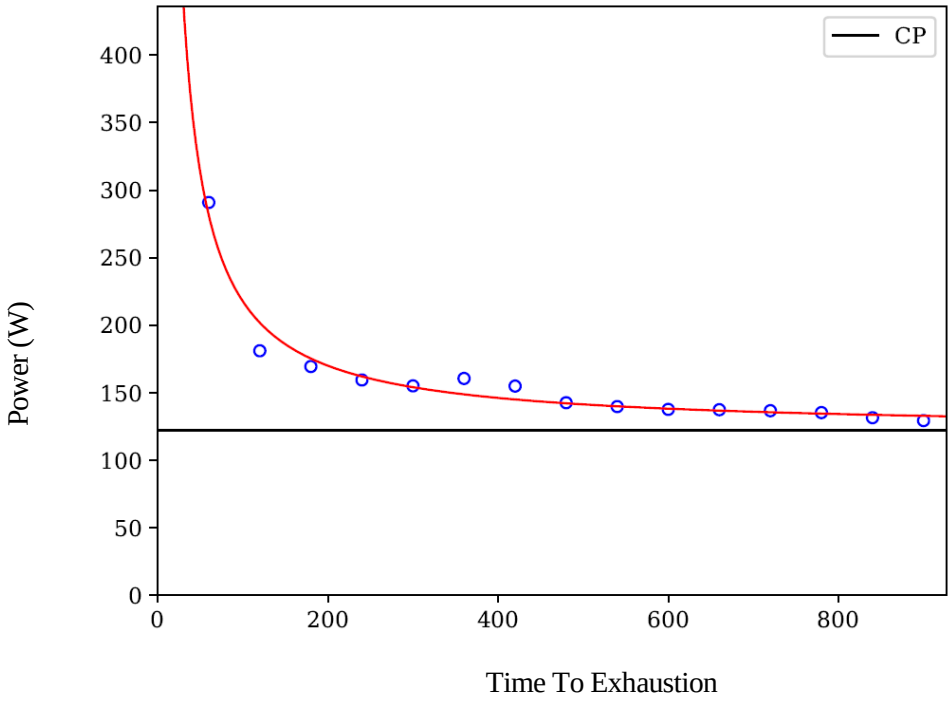

a)

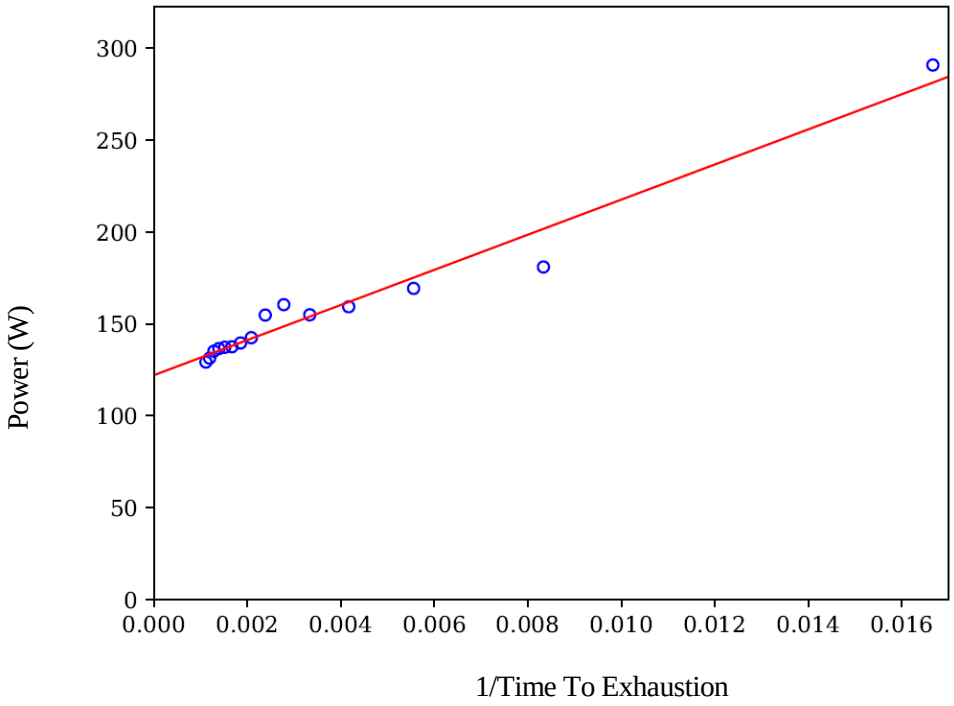

b)

Figure 2. Power Time Relationships for Cyclist 8

2.4. Deceleration Model Development

We extracted a total of 47 deceleration profiles from the dataset. We started by investigating the speed-time relationship. We found that there is always a strong correlation, with $R^2 > 0.98$. This suggests that there is almost a constant deceleration rate, which is equal to the slope of the speed-time relationship. Obviously, cycling deceleration rate depends on the initial speed. The faster a cyclist is traveling, the higher the deceleration rate will be. We used the *curve_fit* method of the Python Scipy Package to fit a power function (9) for the deceleration rate. We found the model had an $RMSE = 0.12$ and the calibrated model parameters were $a = 0.17$ and $b = 0.299$. Figure 3 shows the relationship between the deceleration rate and initial speed for different deceleration profiles and the fitted function.

$$a^{dec}(t) = a \times v_i^b \quad (9)$$

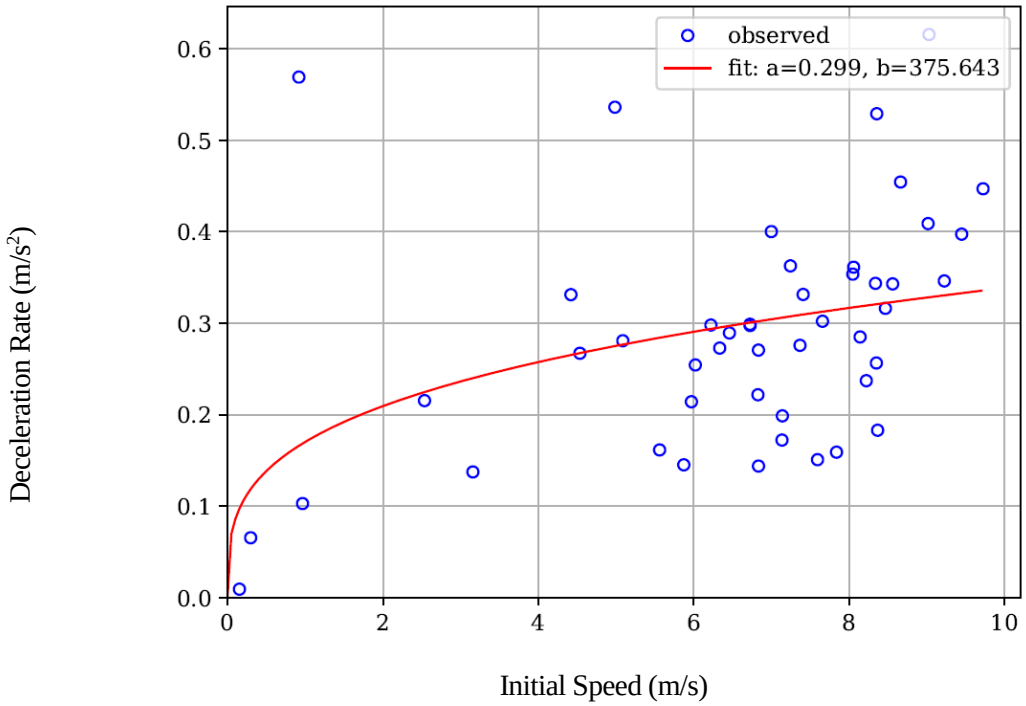

Figure 3. Deceleration Rate Variation as a Function of Initial Speed

2.5. Conclusion and Future Work

In this chapter, we developed a dynamics-based cycling acceleration model that captures cyclist aggressiveness. We augmented the model by calibrating the maximum power for average cyclists. We also developed a model that captures cyclist deceleration behavior. As part of future efforts, we plan to build a high-fidelity microscopic cycling simulation framework that implements these models. We will continue this research using other datasets that could provide more empirical data. We will also study how the calibrated parameters depend on cyclist characteristics, such as gender and age.

3. A Rail Transit Simulation System for Multi-modal Energy-efficient Routing Applications

This chapter develops a continuous rail transit simulator (RailSIM) intended for multi-modal energy-efficient routing applications. RailSIM integrates sophisticated train dynamics and energy models to replicate train motion and energy consumption behavior, respectively. The simulator is calibrated using an off-line optimization procedure to match pre-programmed railway schedules by optimizing three model parameters: segment target speed, average deceleration level, and brake force adjustment factor. The objective of the calibration procedure is to match the simulated and actual average running speed for each station-to-station pair. Upon calibration, RailSIM was applied to the Greater Los Angeles area and validated at both the instantaneous and aggregated levels. Results demonstrate that RailSIM is able to produce realistic train dynamics and energy consumption estimates producing a comfortable ride while simultaneously matching the railway schedule. RailSIM was also demonstrated to capture the sensitivity of energy outputs to the track gradient. Finally, the results indicate that a perfect match to empirical energy estimates is achieved at an average grade of 1.8%, which is a reasonable approximation of the average track gradient of the testing area.

The rest of the chapter proceeds as follows. Section 3.1 provides a synthesis of the related literature on rail simulation. Section 3.2 develops the RailSIM modeling framework, followed by a case study in Section 3.3. Finally, Section 3.4 provides the concluding remarks of the study and several proposed future endeavors.

3.1. Related Work

Urban rail transit operations are complicated and difficult to model. Simulation is a powerful tool to conduct complex rail planning, operations, and control strategies. Extensive efforts in rail simulation have been made to support sustainability of rail operations. Based on the level of simulation detail, railway simulation models can be classified into two categories: discrete and continuous.

Discrete simulation models the operation of a system as a discrete sequence of events over time, and has been widely investigated given that it can be modeled more easily and typically runs faster compared to continuous simulation, which continuously tracks the system dynamics over time. The authors of [18] developed a discrete-event simulation model to analyze transit planning and operation of the central subway portion of the Boston Green Line light rail system. Work in [19] focused on designing an object-oriented approach to discrete-event simulation in support of developing subway timetables and on-line control strategies. In [20], the authors implemented a discrete simulation model to capture operations of both a single terminal and an entire rail network (two or more interconnected terminals). In [21], a discrete event-based simulator for real-time railway traffic management was designed. Discrete simulation was also applied in [22] to replicate train movement and energy consumption. Other discrete models, such as [23], were developed for rail transit simulation. However, these simulation models are not suitable for applications to operational control and optimization associated with energy consumption, given that they are incapable of adequately capturing instant train movements that significantly affect resulting energy estimates. More train motion details are thus needed for energy-efficient applications.

Continuous simulation tracks the system dynamics instantaneously and thus is able to replicate transient train motion. A typical tool, known as OpenTrack, was developed in [24], in which the authors designed a mixed discrete-continuous simulation process and provided a microscopic platform

for railway simulation. OpenTrack successfully achieves a trade-off between running efficiency and simulation detail. Other hybrid simulation systems such as [25, 26] are also operated at either the macroscopic or microscopic level as required by simulation detail. In [27], the authors initiated a continuous microscopic subway simulation system (SimMetro), which was specifically designed to simulate metro rail at the operational level. Those simulation packages, however, cannot adequately replicate train dynamics given the inadequate assumptions of throttle control. For example, [24] assumed that a train always accelerated at full throttle, which overestimates overall acceleration levels.

More sophisticated simulation tools have recently been initiated to replicate details of train movement and energy consumption, such as the train energy and dynamics simulator (TEDS) [28], train dynamics and energy analyser/train simulator (TDEAS) [29], the Centre for Railway Engineering Longitudinal Train Simulator (CRE-LTS) [30], and TrainDy [31]. These tools not only track instant train motion continuously, but also offer more sophisticated functionalities, such as analyzing derailments and slack action. Most of these tools, however, are not open source and thus are difficult to integrate with complex frameworks (i.e., traffic simulation software) to serve higher-level multi-modal transportation planning and management.

RailSIM is anticipated to communicate with other simulation layers (i.e., vehicle, pedestrian, and bike) in real-time, and to support like-for-like comparisons of trip energy consumption among competing travel modes for multi-modal eco-routing applications.

3.2. RailSIM Modeling Framework

The proposed RailSIM framework is a continuous microscopic simulation system designed specifically for multi-modal energy-efficient transportation planning and management. The system consists of four major modules, including an input module, train dynamics and energy consumption models, a calibration procedure, and a simulation module. Figure 4 presents the general architecture of the system. The embedded dynamics model is used to replicate train motions, and the energy model serves to provide energy consumption profiles. The main inputs of the system (i.e., train specifications, passenger ridership, railway schedule, track characteristics, and weather information) are first imported to the calibration procedure in order to determine system unknown parameters, including the segment target speed, average deceleration levels, and brake force adjustment factors[1]. As a follow-up, calibration results along with the main inputs are imported to the simulation module, which instantly outputs trajectories and energy consumption.

3.2.1. Main inputs

RailSIM requires numerous inputs, some of which are readily available, and some of which need to be calibrated. The main inputs of the system can be obtained from transit agencies, websites, or the literature.

Train specifications characterize technical features of a train, including the empty car weight, the number of railcars per train, the train drag coefficient, the number of axles and seating capacity per railcar, the maximum hotel load, and the braking rigging leverage ratio. Most of these inputs can be obtained from transit agencies, with the exception of the braking leverage ratio, which is attainable in the literature.

[1] The brake force adjustment factor is applied to determine the brake level.

Passenger ridership is an important parameter for railway planning, management and operation, and can be modeled at various levels of detail depending on available data. Origin-destination flows of passengers are the typical data used to estimate ridership. However, demand data is sometimes not available. In this case, ridership can be roughly approximated based on annual average passenger loading data, which is readily available in the National Transit Database (NTD). Ridership in this study is used to calculate the passenger weight as a portion of train loading to estimate trip energy consumption.

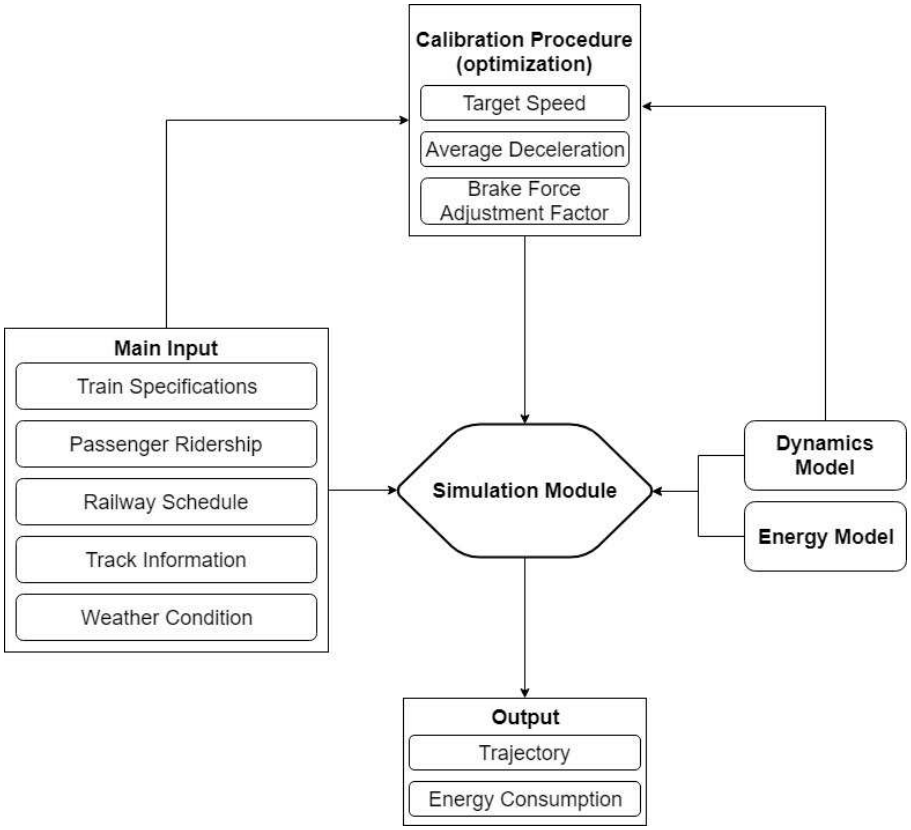

Figure 4. Architecture of RailSIM

The railway schedule provides the arrival and departure times of a train at each station. Basically, the information in a timetable consists of the rail line number/name, driving direction, stop name, arrival and departure time at each stop, and the distance between stations. The timetable of a railway system is typically available online (General Transit Feed Specification [GTFS][2]) or could be procured from transit agencies. Track characteristics (i.e., track type and condition) and weather conditions (i.e., air temperature and humidity) are used to determine the starting tractive effort of a train, which is the additional force required to move the train from a complete stop.

[2] The General Transit Feed Specification (GTFS) defines a common format for public transportation schedules and associated geographic information.

3.2.2. Dynamics and Energy Consumption Modeling

Dynamics Model

Longitudinal dynamics behavior characterizes the motion of rolling stock vehicles in the direction of the track and controls instant vehicle movement. The modeling framework was developed and tested in [32], which modeled train acceleration and deceleration behavior, respectively.

Equation (10) presents the acceleration modeling framework, which estimates dynamics as a function of the tractive force (F_t), resistance force (R), and railcar mass (m). It is worth mentioning that, unlike the trains propelled by a single locomotive, metro rail typically uses Electric Multiple Units that enclose electric traction motors within each railcar for car self-propelling. Consequently, the vehicle acceleration (a) is computed as the resultant force divided by the mass per railcar rather than by total train mass, as illustrated in equation (10.1).

The tractive force varies as a function of the throttle level (λ) and speed (u), constrained by the maximum tractive effort ($\mu\, m_{ta}\, g$), as formulated in equation (10.2). The resistance force consists of the rolling, grade, curving and aerodynamic resistances, and is mathematically characterized by equation (10.3). Details of model parameters can be found in Appendix A.

$$a(t) = \frac{F_t(t) - R(t)}{m} \tag{10.1}$$

$$F_t(t) = \min(3600\,\eta\lambda(t)\frac{P_{max}}{(u(t)\ \times 1.61}, \mu\, m_{ta}\, g) \tag{10.2}$$

$$R(t) = \left[\left(0.6 + \frac{20}{\omega_p} + 0.01\,u(t) + \frac{K\,u(t)^2}{\omega_p n_p} + 20\theta\right)\right] \times \frac{M}{1000} \times 4.4482 \tag{10.3}$$

$$\lambda(t) = \begin{cases} \dfrac{\dfrac{u(t)}{u_d}}{t_1 + \dfrac{t_2}{1 - \dfrac{u(t)}{u_d}} + t_3\dfrac{u(t)}{u_d}}, 0 \le u \le u_m \\ \max\left(\dfrac{\dfrac{u(t)}{u_d}}{t_1 + \dfrac{t_2}{1 - \dfrac{u(t)}{u_d}} + t_3\dfrac{u(t)}{u_d}}, \lambda^*\right), u_m \le u \le u_d \end{cases} \tag{10.4}$$

$$\frac{\min\left(3600\,\eta\,\lambda^*\frac{P_{max}}{u_d \times 1.61}, \mu\, m_{ta}\, g\right) - R}{m} = 0 \tag{10.5}$$

Noticeably, the throttle level, as formulated in equation (10.4), varies as a function of the ratio of the running speed to the desired speed (u_d), rather than being a constant as assumed by the literature [10, 33-35]. An empirical study on light-duty vehicle dynamics modeling, as illustrated in Figure 5, demonstrated a hyperbolic throttle function, implying that drivers push the gas pedal aggressively at

the beginning and gradually release the pedal as the speed approaches the desired speed [11]. u_m in the function is the running speed at the maximum throttle, where the throttle level starts to decrease, and can be estimated based on the ratio of the running speed to the desired speed at the maximum throttle level (α_m, calibrated in [32]). λ^* is the minimum throttle that maintains free driving as demonstrated in (10.5). The throttle function was applied to model electric trains in [32], and was demonstrated to adequately replicate train dynamics behavior.

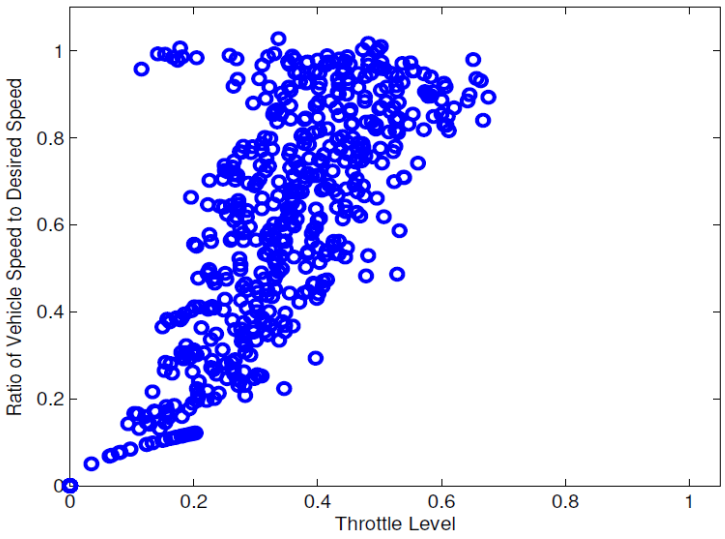

Figure 5. Throttle Level Varies with the Ratio of Current Speed to Desired Speed

The deceleration model, alternatively, characterizes deceleration as a function of the brake force (F_b), resistance and mass per railcar, as illustrated in (11.1). The brake force function, as formulated in (11.2), was first proposed by [36] and further developed in [32], where ω_b is the braking ratio (constant for passenger trains), e is the efficiency of the brake lever system (90–95%), and f is the coefficient of friction between the wheel and the brake shoe varying as a piecewise function of velocity as shown in (11.3). u_1, u_2, Θ, β in (11.3) are model parameters that were calibrated in [32]. Using Equations (11.2) and (11.3), the effect of running speed on the brake force can be explained by the coefficient of friction f varying with velocity.

$$a_d(t) = \frac{F_b(t) - R(t)}{M} \tag{11.1}$$

$$F_b = \omega_b W e f \tag{11.2}$$

$$f(t) = \begin{cases} \Theta u(t), 0 \le u(t) < u_1 \\ \Theta u_1, u_1 \le u(t) < u_2 \\ \Theta u_1 e^{-\beta(u(t)-u_2)}, u(t) \ge u_2 \end{cases} \tag{11.3}$$

Energy Consumption Model

Metro rail is typically powered by electricity. The electric power model used in this study was developed in [37], which characterizes energy consumption/regeneration as piecewise functions, as demonstrated in (12). Equation (12.1) estimates the energy consumed by the tractive effort and

auxiliary systems (i.e. air conditioner, lighting, and ventilation), and Equation (12.2) predicts the energy regenerated during braking. The tractive power P is a function of the tractive force ($F_t + F_s$)[3] and speed. The energy regenerative efficiency (η_{re}) is estimated as an exponential function of the deceleration level as illustrated in (12.4), implying that aggressive braking results in more energy recovered.

The tractive force (F_t) in (12.3) is estimated using (10.2) and only addresses the tractive effort exerted to move the train while in motion. The starting tractive effort (F_s) required to move a train from a complete stop is determined based on track characteristics and weather conditions. For more energy model details, readers are referred to [37].

$$EC(t) = \begin{cases} HEP + P(t), \forall P(t) > 0 \\ HEP, \quad \forall P(t) \leq 0 \end{cases} \tag{12.1}$$

$$EC_{re}(t) = \begin{cases} P(t) \times \eta_{re}(t), \forall P(t) < 0 \\ 0, \quad \forall P(t) \geq 0 \end{cases} \tag{12.2}$$

$$P(t) = \frac{1.6 \times (F_t + F_s) \times u}{3600 \times \eta} \tag{12.3}$$

$$\eta_{re}(t) = \begin{cases} \dfrac{1}{\dfrac{\gamma}{e^{|a(t)|}}}, \forall P(t) < 0 \\ 0, \quad \forall P(t) \geq 0 \end{cases} \tag{12.4}$$

3.2.3. Calibration Procedure

As previously mentioned, some of the simulation inputs are not readily available and need to be calibrated. Specifically, three parameters remain to be determined, including the segment target speed, the average deceleration level, and the brake force adjustment factor. It is worth noting that these parameters should be calibrated for each of the track segments connecting two neighboring stations (station-to-station pairs). The target speed is the maximum speed that a train is allowed to reach on each segment in order to meet its schedule. The average deceleration level is used to determine where a train should start to decelerate to ensure a complete stop upon arrival at the next station. The brake force adjustment factor serves to determine the level at which the brake force varies with running speed. Specifically, **Error! Reference source not found.** presents the dynamic brake characteristics o f electric locomotives, which characterizes the braking force as a piecewise function of speed at multiple discrete levels [38]. However, Equation (11.1) is not able to capture the discrete feature. For simplicity, an adjustment factor (ω_a) was introduced to the brake force model (11.2) to determine the discrete level applied to each segment. Larger ω_a will result in higher discrete levels.

[3] F_s is the starting tractive effort required to move a train from a complete stop; it equals 0 when the train is moving.

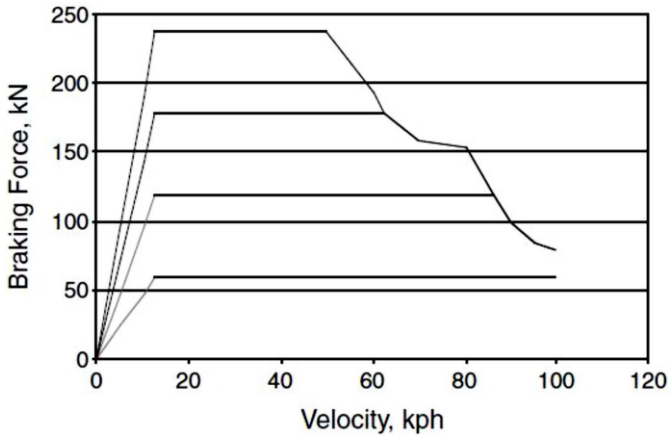

Figure 6. Dynamic Brake Characteristics of Electric Trains

The calibration effort is formulated as a non-linear optimization problem, as demonstrated in (13) Consider a rail line that consists of κ station-to-station pairs (κ track segments), T_k and $\bar{u}_k$ refer to the actual travel time and average speed on segment k derived from the timetables, respectively; $\hat{u}_k$ is the simulated instantaneous speed; E_k is the simulation error of the average running speed compared to the real-world value on segment k; $\hat{a}_k$ and $\bar{x}_k$ are the simulated acceleration and distance respectively; $u_{d,k}$ is the segment-specific target speed; U_{max} is the maximum allowed running speed of a railway system; $\bar{a}_{d,k}$ is the average deceleration on segment k; $\omega_{a,k}$ is the segment-specific brake force adjustment factor, $W_{a,k}$ is the solution set of $\omega_{a,k}$, and $\omega_{optimum}$ is the optimum solution of $\omega_{a,k}$; Δt is the time interval (1 s used in this study); f_{max} is the maximum coefficient of friction determined by (11.3) ($f_{max} = \alpha u_1$)

The objective of the optimization problem is to minimize the simulation error of the average speed on each track segment while satisfying the constraints (13.2-13.9). Constraints (13.2) and (13.3) ensure that the estimated speeds and distances satisfy the system of the first-order ordinary differential equations in addition to the non-negativity constraint (13.8), and that the running speed does not exceed the target speed. Constraint (13.4) ensures that target speed does not exceed the maximum allowed speed and is greater than the average speed[4]. Constraint (13.5) provides the average deceleration level search window, which is determined based on engineering intuition that aggressive deceleration should be avoided as much as possible to ensure ride comfort and safety. Constraint (13.6) indicates that the adjusted brake force should be smaller than the maximum allowed brake force ($\mu m_{ta} g$).

Also, there may be multiple ωa,k solutions to the problem ($W_{a,k} = (\omega^1_{a,k}, \omega^2_{a,k}, \omega^3_{a,k}, \ldots)$), and the solutions with the minimum $\omega_{a,k}$ would be taken as the optimum solutions as described by the constraint $\omega_{a,k}^{optimum} = \min(W_{a,k})$, given that a lower brake force achieves milder deceleration for ride safety and comfort. Constraint (13.7) guarantees a complete stop upon arrival at a station. Constraint (13.9) ensures that simulated- and actual- average speeds match exactly.

$$\min_{k=1,2,\ldots,\kappa} E_k = \left(\frac{\sum_{t=0}^{T_k} \hat{u}_k(t)}{T_k} - \bar{u}_k \right)^2 \qquad (13.1)$$

[4] The target speed should be greater than average speed to guarantee that the simulated average speed is not less than the real value.

$$s.t.: \hat{u}_k(t) = \min(\hat{u}_k(t-1) + \hat{a}_k(t)\Delta t, u_{d,k}) \quad (13.2)$$

$$\hat{x}_k(t) = \hat{x}(t-1) + \hat{u}_k(t)\Delta t \quad (13.3)$$

$$\bar{u}_k \leq u_{d,k} \leq U_{max} \quad (13.4)$$

$$0.1 \leq \bar{a}_{d,k} \leq 2.0 \quad (13.5)$$

$$1.0 \leq \omega_{a,k} \leq \frac{0.45\,\mu\, m_{ta}\, g}{4.4482\,\omega_b emf_{max}}, \omega_{a,k}^{optimum} = \min(W_{a,k}) \quad (13.6)$$

$$\hat{u}_k(T_k) = 0 \quad (13.7)$$

$$\hat{u}_k(t), \hat{x}_k(t) \geq 0 \quad (13.8)$$

$$E_k = 0 \quad (13.9)$$

These equations comprise the procedure to solve the optimization problem. Basically, the simulation model is calibrated segment-by-segment. For each of the segments k, the procedure first initializes the simulation error to be a large number to proceed (E_k = 10, 000 is used here), and then calculates the passenger loading, the number of cars per train (N), the seating capacity (C_s), the car mass (m), and total train mass (M), which are used to estimate acceleration and the forces acting on a train. Calibration work starts from an initialization procedure that assumes that a train departing from a station accelerates from a complete stop ($\hat{u}(0) = 0$) at the initial position ($\hat{x}(0) = 0$). For all control variables ($u_{d,k}$, $\bar{a}_{d,k}$, and $\omega_{a,k}$), acceleration, vehicle speed, location, and acting forces are calculated for each observation t. It is worth noting that the deceleration distance (L_d) is estimated to determine the moving status of a train: acceleration, cruise or deceleration. D_k in the table refers to the length of segment k (namely, the distance between two neighboring stations). For each set of control variables, the simulation error (E_k) is calculated. The optimal solutions ($u_{d,k}^{optimum}$, $\bar{a}_{d,k}^{optimum}$, $\omega_{d,k}^{optimum}$) should be those that guarantee that the simulated- and actual- average speeds match exactly ($E_k = 0$) and ensure a complete stop upon arrival at the next station ($\hat{u}(T_k) = 0$), while at the same time achieve the minimum brake force adjustment factor. Noticeably, for some of the track segments, railway schedules may not be correct, resulting in extremely high actual average speeds (higher than the maximum allowed running speed U_{max}). The calibration algorithm provides an error check procedure by introducing a while loop that could trigger the increase of travel time ($T_k = T_k+1$) on segment k for re-calibration if $E_k > 0$ at the end of the last calibration, and the procedure ends when $E_k = 0$.

3.2.4. Simulation Module

The calibration procedure presented in Table 3 is essentially an off-line calibration of the model parameters for use as input to the simulation module. Simulation inputs broadly include train specifications, passenger ridership, the railway schedule, calibration parameters, track information, and weather conditions.

Table 4 describes the work flow of the simulation module. Similar to the calibration procedure, the simulation module also runs segment-by-segment. For each of the track segments k, the module first estimates the passenger loading, the number of railcars per train (N), the seating capacity (Cs), the railcar mass (m), and total train mass (M), all of which vary with rail line; running direction; and time

of operation (peak vs. non-peak hours). The deceleration distance is also calculated to determine the moving status of a train. The simulation run starts with an initialization procedure and generates the simulation results for each observation t, including speed, acceleration, and energy consumption.

3.3. Case Study: Los Angeles Metro Rail Transit

In this section, RailSIM is applied to the Los Angeles (LA) rail transit network. The LA Metro rail is an urban rail system serving Los Angeles County, California. There are six rail lines, including two rapid transit subway lines (Red and Purple) and four light rail lines (Blue, Gold, Green and Expo)[5], serving 95 stations and covering 105 mi of track. The six lines are marked with a number from 801 to 806. All rail lines run regularly between 5 a.m. and midnight, seven days a week. Peak and off-peak operation hours differ among rail lines and between moving directions. The rolling stocks in the LA metro rail are all electric-powered.

Table 3. Calibration Procedure of the Simulation Model

PROCEDURE

for all track segment κ ***do***

initialize $E_k = 10000$

Determine $passenger\ loading, number\ of\ railcars\ per\ train\ (N),$

$seating\ capacity\ (C_s), m, M$

While $E_k > 0$ **do**

$Inintialization\ \hat{u}(0) = 0, \hat{x}(0) = 0\ \rightarrow \lambda, F_t(0), R(0)$

for all $u_{d,k}, u_{d,k} \in |\bar{u}_k, U_{max}|$ **do**

for all $\bar{a}_{d,k}, \bar{a}_{d,k} \in 0.1, 0.2, \dots, 2.0$ **d**

Decelration distance: $L_d = \frac{u_{d,k}^2}{2\bar{a}_{d,k}}$

for all $\omega_{a,k}, \omega_{a,k} \in \left|1.0, \frac{0.45\ \mu\ m_{ta}\ g}{4.4482\omega_b emf_{max}}\right|$ **do**

for all $observations\ t \leftarrow 1, 2, \dots, T_k$ **do**

if $u_{d,k} - \hat{u}(t-1) > 0$ and $D_k - \hat{x}(t-1) > L_d$ **then**

Acceleration: $\hat{a}(t) = \frac{F_t(t-1) - R(t-1)}{m}$

$\hat{u}(t) = \hat{u}(t-1) + \hat{a}(t)\Delta t, \hat{u}(t) = \min(\hat{u}(t), u_{d,k})$

[5] The orange line is a metro bus line.

PROCEDURE

$\hat{x}(t) = \hat{x}(t-1) + \hat{u}(t)\Delta t$

Throttle function $\rightarrow \lambda$

Calculate F_t, R

else if $u_{d,k} - \hat{u}(t-1) = 0$ and $D_k - \hat{x}(t-1) > L_d$ **then**

Cruise: $\hat{a}(t) = 0, \hat{u}(t) = \hat{u}(t-1)$

$\hat{x}(t) = \hat{x}(t-1) + \hat{u}(t)\Delta t$

Calculate F_t, R

else if $D_k - \hat{x}(t-1) \leq L_d$ **then**

Deceleration: Brake force function $\rightarrow f, F_b, R$

$$\hat{a}(t) = \frac{F_t(t) + R(t)}{m}$$

$\hat{u}(t) = \hat{u}(t-1) - \hat{a}(t)\Delta t$

$\hat{x}(t) = \hat{x}(t-1) - \hat{u}(t)\Delta t$

end if

end for

end for

end for

end for

if $E_k > 0$ **the**

$T_k = T_k + 1$

else

break

end if

end while

Find all solutions with $\hat{u}(T_k) = 0$ that minimize $E_k (E_k = 0)$

Select the solutions with the minimum $\omega_{a,k}$ as the final solution

PROCEDURE

$(u_{d,k}^{optimum}, \bar{a}_{a,k}^{optimum}, \omega_{a,k}^{optimum})$

end if

end PROCEDURE

Table 4. Simulation Module

PROCEDURE

Input: main inputs plus calibration results $(u_{d,k}^{optimum}, \bar{a}_{a,k}^{optimum}, \omega_{a,k}^{optimum})$

for all κ **do**

Determine $passenger\ loading, number\ of\ railcars\ per\ train\ (N),$

$seating\ capacity\ (C_s), m, M$

Deceleration distance: $L_d = \frac{\left(u_{d,k}^{optimum}\right)^2}{2\bar{a}_{d,k}^{optimum}}$

Initialization $\hat{u}(0) = 0, \hat{x}(0) = 0 \rightarrow \lambda(0), F_t(0), R(0)$

for all observations $t \leftarrow 1, 2, \ldots, T_k$ **do**

if $u_{d,k} - \hat{u}(t-1) > 0$ and $D_k - \hat{x}(t-1) > L_d$ **then**

Acceleration: $\hat{a}(t) = \frac{F_t(t-1) - R(t-1)}{m}$

$\hat{u}(t) = \hat{u}(t-1) + \hat{a}(t)\Delta t, \hat{u}(t) = \min(\hat{u}(t), u_{d,k}$

$\hat{x}(t) = \hat{x}(t-1) + \hat{u}(t)\Delta$

Throttle Function $\rightarrow \lambda$

Estimate $F_t, R,$ and energy consumption (EC)

else if $u_{d,k} - \hat{u}(t-1) = 0$ and $D_k - x(t-1) > L_d$ **then**

Cruise: $\hat{a}(t) = 0, \hat{u}(t) = \hat{u}(t-1)$

$\hat{x}(t) = \hat{x}(t-1) + \hat{u}(t)\Delta t$

Estimate $F_t, R,$ and energy consumption (EC)

else if $u_{d,k} - \hat{u}(t-1) = 0$ and $D_k - x(t-1) > L_d$ **then**

PROCEDURE

Deceleration: Brake force function $\rightarrow f, F_b, R$

$$\hat{a}(t) = \frac{F_b(t) + R(t)}{m}$$

$$\hat{u}(t) = \hat{u}(t-1) - \hat{a}(t)\Delta t, \hat{x}(t) = \hat{x}(t-1) + \hat{u}(t)\Delta t$$

Estimate F_b, R, and energy consumption/regeneration (EC and EC_{re})

end if

end for

end for

end PROCEDURE

3.3.1. RailSIM Inputs

The inputs to the simulation model are classified into two categories: static and dynamic. Static inputs do not vary with track segment and time of operation, and thus are assumed to be constant, including parameters of dynamics and energy consumption models, track and weather conditions, and some of the rolling stock parameters[6]. Dynamic inputs refer to the variables that vary as a function of rail line, moving direction, and time of operation. Static inputs were obtained mainly from either LA Metro or from the literature, as illustrated in Table 5, which describes the details of the parameter values and sources. Specifically, LA Metro provided the maximum head-end power (HEP) information, track conditions, number of axles per railcar (n_p), maximum allowed running speed (U_{max}) of the LA rail system, and maximum traction power (P_{max}) of the LA rolling stocks. Weather conditions were assumed to be dry (typical weather conditions in California), and atmospheric temperature was considered normal. Other parameters were determined from the literature. It is worth mentioning that a unit passenger weight of 68 kg was suggested according to the literature, given a lack of data on the actual weight of each individual passenger [37, 39, 40].

Dynamic variables include the information provided in the railway schedule and the rolling stock parameters that vary with rail line, moving direction, and time of operation. Table 6 gives an example of the LA Metro rail schedule (derived from the GTFS file), which provides the route ID, moving direction ID, trip ID, arrival and departure time at each station, station ID, sequence, name, location (longitude and latitude), and the distance for each station-to-station pair. Travel time and average speeds in the table were estimated based on the given distances and arrival/departure times. There are two trips in the table with different moving directions (direction ID of 0 for south or west, and 1 otherwise). Both trips are on rail line 804 (the Gold line). Trip 1 starts from the Sierra Madre Villa Station and ends at the Little Tokyo/Arts District Station, and Trip 2 starts from the Atlantic Station

[6] Some of the rolling stock parameters are considered static inputs. These include the drag coefficient and maximum hotel load, while some are dynamic, such as the number of cars per train and weight per railcar, which depend on the rail line, moving direction, and time of operation.

and ends at the Union Station.

Table 7 describes the rolling stock parameters that vary with rail line, moving direction, and/or operation hours. Specifically, seating capacity and empty car weight depend on rail line only. The number of railcars per train, alternatively, differs between peak and off-peak hours which vary with rail line and moving direction. Noticeably, there are no off-peak hours on Line 805, demonstrating that this line is always busy during operation hours. In addition, LA Metro provided the number of passengers boarding and alighting per station on an hourly basis to estimate passenger loading.

3.3.2. RailSIM Calibration for LA Metro Rail

As previously noted, calibration of the simulation model can be mathematically characterized as an optimization problem that attempts to match the simulated- and actual- average speeds for each station-to-station pair. Based on the calibration procedure presented in section 3.2.3, three control parameters were calibrated: the target speed, the average deceleration level, and the brake force adjustment factor. The target speed was increased by 1.0 mi/hour at each step within the search window [$\bar{u}_k$, U_{max}], and average deceleration was varied at steps of 0.1 m/s^2 within a [0.1, 2.0] window. The brake force adjustment factor varied at increments of 0.5 within the search window [1.0, $\frac{0.45\ \mu\ m_{ta}\ g}{4.4482\ \omega_b\ emf_{max}}$]. The use of 0.5 not only ensures the existence of optimal solutions, but averts computational exhaustion resulting from the small step size. It should be noted that, for 10% of station-to-station pairs, the actual average speeds are higher than the maximum allowed running speed U_{max}, resulting in an unfeasible schedule. For these segments, we reduced the dwell time at the destination station and allowed the train's arrival time to be delayed up to 30% (with an average delay of 7 s) to maintain the schedule.

Table 5. RailSIM Static Inputs

Parameter	Value	Source
Maximum HEP per railcar	60 (KW)	LA Metro
Track Type	115 lb (52 kg) rail	LA Metro
Track condition	Good rails and crossties	LA Metro
n_p	6	LA Metro
U_{max}	50 (mi/hr)	LA Metro
P_{max}	580 (kW)	LA Metro
Air temperature	25 °C (Normal temperature)	-
Weather condition	Dry	-
Unit passenger weight	68 (kg)	[39]
K	0.07	[41]
η	0.9	[32]
μ	0.2	[32]
ω_b	0.9	[32]

Parameter	Value	Source
γ	0.65	[37]
Dynamic model parameters	$\alpha_m = 0.55$	[32]
	$t_1 = 0.05$	[32]
	$t_2 = 0.1012$	[32]
	$\alpha = 1/46$	[32]
	$u_1 = 6$	[32]
	$u_2 = 21$	[32]
	$\beta = 0.1$	[32]

The calibration effort generated the optimum control variables for each track segment. As an example, Table 8 presents the calibration results for the two trips described in Table 6. Specifically, the optimal solutions (optimum target speed, average deceleration level, and brake force adjustment factor) are different among the segments given the different arrival/departure times and distances. An error of 0 demonstrates the exact match between the simulated- and real-average speeds. All six rail lines were calibrated with the simulation error of 0, demonstrating that the proposed calibration approach is able to adequately model LA train movements while simultaneously matching railway schedules.

Table 6. Los Angeles Metro Rail Schedule (Example Schedule for Line 804)

Dir.	Trip ID	Arrival Time	Dep. Time	Stop ID	Stop Seq.	Stop Name	Distances (*mi*)	Arrival time	Dep. Time	Travel Time (s)	Ave. Speed (mi/hr
1	38882065	24:58:00	24:58:00	80421	1	Sierra Madre Villa Station	1.99	89880	89880	160	45
1	38882065	25:00:40	25:01:00	80420	2	Allen Station	0.98	90040	90060	100	35
1	38882065	25:02:40	25:03:00	80419	3	Lake Station	1.07	90160	90160	100	39
1	38882065	25:04:40	25:05:00	80418	4	Memorial Park Station	0.45	90280	90300	40	41
1	38882065	25:05:40	25:06:00	80417	5	Del Mar Station	0.58	90340	90360	100	21
1	38882065	25:07:40	25:08:00	80416	6	Fillmore Station	1.49	90460	90480	160	34
1	38882065	25:10:40	25:11:00	80415	7	South Pasadena Station	2.12	90640	90660	220	35
1	38882065	25:14:40	25:15:00	80414	8	Highland Park Station	1.3	90880	90900	160	29
1	38882065	25:17:40	25:18:00	80413	9	Southwest Museum Station	0.89	91060	91080	100	3
1	38882065	25:19:40	25:20:00	80412	10	Heritage Square/Arroyo Station	0.6	91180	91200	100	22
1	38882065	25:21:40	25:22:00	80411	11	Lincoln Heights/Cypress Park Station	1.55	91300	91320	160	35
1	38882065	25:24:40	25:25:00	80410	12	Chinatown Station	0.62	91480	91500	100	22
1	38882065	25:26:40	25:27:00	80409	13	Union Station-Metro Gold Line	0.54	91600	91620	220	9
1	38882065	25:30:40	25:31:00	80408	14	Little Tokyo/Arts District Station	0.76	91840	91860	0	0
0	38882083	24:03:00	24:03:00	80401	1	Atlantic Station	0.39	86580	86580	100	14
0	38882083	24:04:40	24:05:00	80402	2	East LA Civic Center Station	0.4	86680	86700	160	9
0	38882083	24:07:40	24:08:00	80403	3	Maravilla Station	1.44	86860	86880	280	19
0	38882083	24:12:40	24:13:00	80404	4	Indiana Station	1.26	87160	87180	160	28
0	38882083	24:15:40	24:16:00	80405	5	Soto Station	0.61	87340	87360	40	55
0	38882083	24:16:40	24:17:00	80406	6	Mariachi Plaza/Boyle Heights Station	0.36	87400	87420	100	13
0	38882083	24:18:40	24:19:00	80407	7	Pico/Aliso Station	0.76	87520	87540	220	12
0	38882083	24:22:40	24:23:00	80408	8	Little Tokyo/Arts District Station	0.54	87760	87780	220	9
0	38882083	24:26:40	24:27:00	80409	9	Union Station-Metro Gold Line	0.62	88000	88020	0	0

Table 7. Rail Line Information of Los Angeles Metro

Route	Dir.	Off-peak Hours	Number of Cars	Seating Capacity	Empty Car Weight (ton)
801	0	0, 1, 2, 21, 22, 23	off-peak: 2, peak: 3	100	44.45
	1	0, 1, 2, 3, 22, 23			
802	0	0, 1, 2, 9, 11, 12, 13, 14, 21, 22, 23	off-peak: 4, peak: 6	180	36.29
	1	0, 1, 10, 11, 12, 13, 14, 22, 23			
803	0	0, 1, 2, 23	off-peak: 1, peak: 2	100	44.45
	1	0, 1, 2, 22, 23			
804	0	0, 1, 2, 21, 22, 23	off-peak: 1, peak: 2	100	44.45
	1	1			
805	0	-	off-peak: 2, peak: 4	180	36.29
	1	-			
806	0	0-23	off-peak: 2, peak: 3	100	44.45
	1	0-23			

Table 8. RailSIM Calibration Results for Los Angeles Metro Rail (Example Result)

Route	Dir.	Trip ID	Stop ID	Stop Seq.	Distances	Arr. Time	Dep. Time	Travel Time	Ave. Speed	Segment Target Speed	Brake Force Average Deceleration	Adj. Factor	Error
804	1	38882065	80421	1	1.99	89880	89880	160	45	50	0.6		0
804	1	38882065	80420	2	0.98	90040	90060	100	35	49	0.3		0
804	1	38882065	80419	3	1.07	90160	90180	100	39	49	0.5		0
804	1	38882065	80418	4	0.45	90280	90300	40	41	46	0.8		0
804	1	38882065	80417	5	0.58	90340	90360	100	21	26	0.8	1	0
804	1	38882065	80416	6	1.49	90460	90480	160	34	44	0.3	1	0
804	1	38882065	80415	7	2.12	90640	90660	220	35	40	0.4	1	0
804	1	38882065	80414	8	1.3	90880	90900	160	29	34	0.5	1	0
804	1	38882065	80413	9	0.89	91060	91080	100	32	41	0.5		0
804	1	38882065	80412	10	0.6	91180	91200	100	22	27	0.8	1	0
804	1	38882065	80411	11	1.55	91300	91320	160	35	44	0.3	1	0
804	1	38882065	80410	12	0.62	91480	91500	100	22	27	0.6	1	0
804	1	38882065	80409	13	0.54	91600	91620	220	9	10	0.3	1	0
804	1	38882065	80408	14	0.76	91840	91860	0	0	0	0		0
804	0	38882083	80401	1	0.39	86580	86580	100	14	17	0.6	1	0
804	0	38882083	80402	2	0.4	86680	86700	160	9	10	0.3	1	0
804	0	38882083	80403	3	1.44	86860	86880	280	19	20	0.9	1	0
804	0	38882083	80404	4	1.26	87160	87180	160	28	32	0.5	1	0
804	0	38882083	80405	5	0.61	87340	87360	40	55	50	0.6		0
804	0	38882083	80406	6	0.36	87400	87420	100	13	15	0.6	1	0
804	0	38882083	80407	7	0.76	87520	87540	220	12	13	0.2	1	0
804	0	38882083	80408	8	0.54	87760	87780	220	9	10	0.3	1	0
804	0	38882083	80409	9	0.62	88000	88020	0	0	0	0	0	0

3.3.3. Simulation Results

Calibration results, along with the main inputs, were imported to the simulation module to generate train trajectories and instantaneous energy consumption levels. An example result output from the simulation of a trip on Line 804 is provided in Figure 7, which gives second-by-second speed, acceleration, jerk, and electric power consumption. The trip continues a total of 1,740 s, which includes dwell times at each station. Departing from a station, the train basically accelerates from a complete

stop to the optimized target speed, and cruises until the location where the train should start to decelerate is reached. Then the train decelerates from the target speed to complete a stop upon arrival at the next station. As illustrated in Figure 7, the resulting acceleration is in a reasonable range ([−2.0, 2.0m/s^3]) and varies as a function of the running speed in a similar way as shown in the literature [11, 32, 34], demonstrating realistic dynamics behavior from RailSIM. In addition, jerk is no greater than 2.0 m/s^3, ensuring a safe and comfortable ride. Finally, RailSIM also provides the instantaneous net energy power to predict trip-level energy consumption.

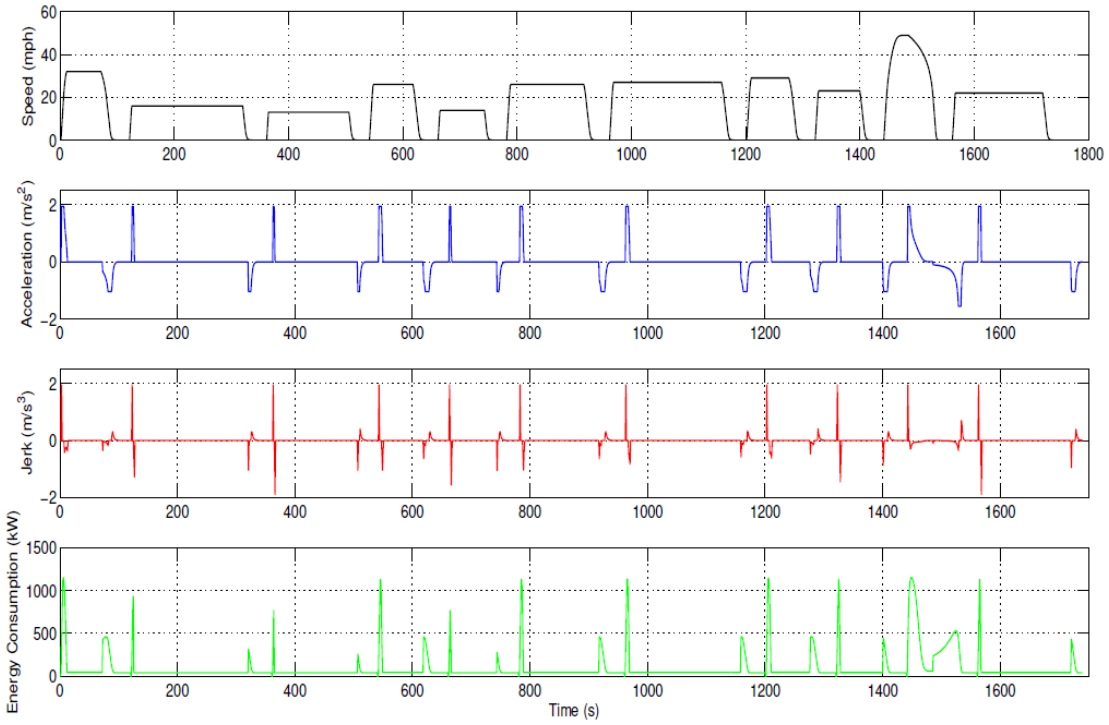

Figure 7. Instantaneous Simulation Results

The simulation was run for all six rail lines, taking approximately 2 mins to complete the run, and demonstrating the simulation model's high running efficiency. The resulting acceleration is in an acceptable range of [−5.2, 2.0m/s^2][7]. More importantly, the maximum jerk for all lines is 3 m/s^3, which guarantees a safe and comfortable ride according to [42], which demonstrated that a jerk of 3 m/s^3 was highly acceptable at low acceleration levels (smaller than 1.0 m/s^2), as illustrated in Figure 8.

[7] The deceleration of 5.2 m/s^2 only occurs on those segments where the actual average speeds are greater than U_{max}; for most of other segments, the deceleration level is no greater than 2.0 m/s^2, as illustrated in Figure 7. .

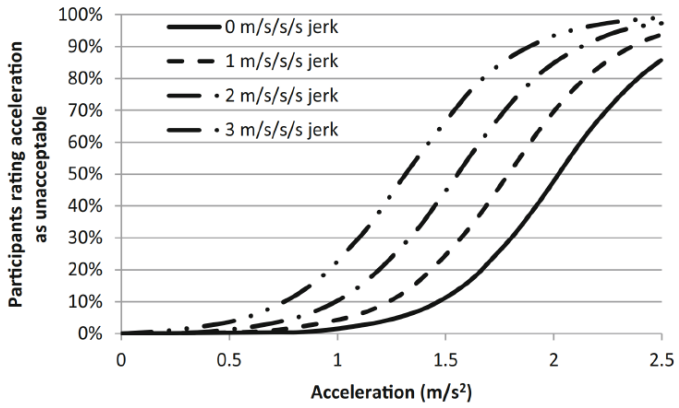

Figure 8. Acceptability of Acceleration/Jerk Levels ([42])

In addition to the instantaneous results, RailSIM was also validated against aggregated data by comparing simulated- and actual- daily energy consumption. Given a lack of instantaneous energy data from LA Metro, daily energy consumption was used for validation purposes. As reported by LA Metro, the railway system consumes a total of 177,375,129 kWh of electric power annually. Assuming that energy is consumed equally every day, the actual daily energy consumption would be 485,959 kWh/day. The instant energy outputs from RailSIM were accumulated on a daily basis to estimate simulated daily energy consumption. It is worth noting that the track gradient was assumed to be 0% while calibrating RailSIM given a lack of gradient data, which is extremely difficult to collect for underground railway systems[8]. The testing effort was thus conducted at multiple track gradient levels varying between 0% and 3%, as illustrated in Table 9. Simulated energy consumption increases considerably—from 287,674.96 to 683,864.91 kWh/day—with the track gradient varying from 0% to 3%. Compared to the actual energy consumption of 485,959 kWh/day, the simulation error first decreases from 40.8% and then increases back to 40.72% with the minimum point of 0.34% at an average grade of 1.8%. Figure 9 illustrates the variation in the energy estimate error as a function of the track gradient with the optimal model estimation at an average grade of 1.8%. This demonstrates that RailSIM is able to significantly reflect the sensitivity of energy simulation results to track gradient. In addition, given the mountainous terrain in the LA area, an approximation of 1.8% to the area-average gradient appears to be reasonable. Consequently, the results seem to demonstrate the validity of the RailSIM framework.

Table 9. Sensitivity of Simulation Results to Track Gradient

Grade (%)	Line Number						Total Daily Energy Consumption (kWh)	Error of Energy Consumption (%)
	801	802	803	804	805	806		
0	82862.98	93520.16	37901.56	25366.52	29754.14	18269.6	287674.96	40.8
0.1	86526.92	96285.61	39707.24	26355.1	30446.21	19041.44	298362.51	38.6
0.2	90102.97	98947.44	41315.2	27337.62	31115.27	19829.81	308648.31	36.49

[8] A significant number of track segments are underground in the LA Metro rail system.

Grade (%)	Line Number						Total Daily Energy Consumption (kWh)	Error of Energy Consumption (%)
	801	802	803	804	805	806		
0.3	93658.82	101656.69	42924.73	28295.63	31722.58	20657.44	318915.89	34.37
0.4	97362.46	104611.03	44686.87	29285.01	32427.09	21454.37	329826.84	32.13
0.5	101000.77	107250.91	46345.89	30287	33050.36	22236.62	340171.53	30
0.6	104598.2	109955.96	48089.59	31291.51	33693.28	23026.15	350654.69	27.84
0.7	108241.42	113008.11	49809.98	32306.8	34456.16	23826.03	361648.5	25.58
0.8	111860.56	115894.79	51548.03	33329.11	35148.09	24610.8	372391.39	23.37
0.9	115710.1	118825	53298.94	34331.39	35865.95	25450.59	383481.99	21.09
1	119314.08	121623.58	55036.05	35330.67	36510.65	26234.42	394049.45	18.91
1.1	123049.22	124631.9	56739.32	36343.41	37337.92	27036.83	405138.59	16.63
1.2	126664.62	127601.64	58472.64	37337.11	38000.27	27829.31	415905.59	14.42
1.3	130620.32	130568.34	60287.25	38425.43	38724.53	28642.97	427268.83	12.08
1.4	134406.03	133810.77	62171.06	39479.39	39562.5	29468.19	438897.94	9.68
1.5	138185.28	136654.45	64002.23	40535.53	40236.57	30266.03	449881.59	7.42
1.6	142041.5	139764.74	65862.77	41534.97	41027.12	31076.01	461308.72	5.07
1.7	145884.59	142819.17	67768.32	42558.72	41762.96	31878.37	472673.84	2.73
1.8	149980.33	145616.4	70052.25	43689.68	42227.6	32725.17	484293.24	0.34
1.9	158760.92	148939.37	79294.72	46185.03	42983.31	33506.37	509669.72	4.88
2	164065.5	152199.33	81391.35	47267.94	43688.17	34298.98	522911.27	7.6
2.1	168929.58	163655.34	83520.86	48417.2	44517.34	35123.64	544163.98	11.98
2.2	173191.03	168946.8	85786.38	49570.24	45242.1	35912.98	558649.53	14.96
2.3	177196.62	172367.77	87890.76	51191.62	46003.33	36731.91	571382.02	17.58
2.4	181408.79	176003.73	90495.79	52307.07	46752.04	37533.99	584501.42	20.28
2.5	185814.54	179528.22	92731.96	53439.27	47610.8	38363.55	597488.33	22.95
2.6	190124.95	185273.57	94921.59	54563.54	50099.25	39218.18	614201.08	26.39
2.7	200448.37	188825.58	99236.76	55779.07	50869.8	40087.74	635247.32	30.72

Grade (%)	Line Number						Total Daily Energy Consumption (kWh)	Error of Energy Consumption (%)
	801	802	803	804	805	806		
2.8	205069.04	192658.65	101495.57	56913.81	51674.06	40913.21	648724.34	33.49
2.9	211578.95	196332.21	103761.2	58066.36	52522.46	41821.15	664082.34	36.65
3	220443.72	199715.72	106056.48	59947.13	53314.84	44387.02	683864.91	40.72

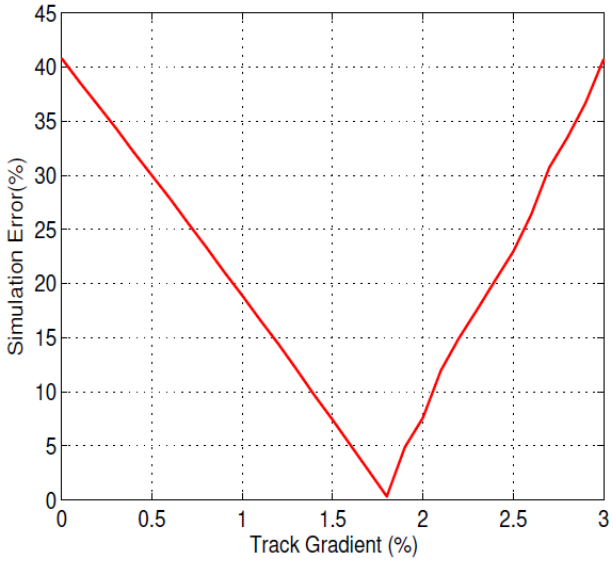

Figure 9. Simulation Error vs. Track Gradient

3.4. Conclusions and Recommendations for Further Research

This chapter presented a novel microscopic rail transit simulator (RailSIM) for use in a multi-modal agent-based modeling system. RailSIM integrates sophisticated train dynamics [32] and energy consumption models [37], enabling continuous modeling of train motion and accurate estimates of energy consumption levels. The simulator was calibrated using an off-line optimization approach to match existing railway schedules by calibrating three segment-specific control variables: the target speed, the average deceleration level, and the brake force adjustment factor. The objective of the calibration procedure was to match the simulated- and actual-average running speeds for each station-to-station pair. A case study was ultimately conducted and the model was validated using the Los Angeles Metro Rail data at both the instantaneous and aggregated levels.

Results demonstrate that RailSIM was able to replicate realistic dynamics behavior and guarantee a comfortable passenger ride while simultaneously matching railway schedules. In addition, RailSIM was demonstrated to significantly reflect the sensitivity of energy simulation results to track gradient. The simulated energy consumption error was found to be close to 0% with a reasonable approximation of the average track gradient. RailSIM will be integrated with other traffic simulation models (i.e., on-road vehicle simulator, pedestrian/bike simulator), and is valuable for multi-modal transportation planning and management applications.

The major limitation of this study is the limited availability of observed trajectory and instantaneous energy consumption data. The authors only had access to the annual aggregated energy consumption reported by Los Angeles Metro as the benchmark of system testing. Consequently, validation of the instantaneous energy consumption is recommended in the future. In addition, it would be interesting to investigate the performance of RailSIM in other rail metro systems. Finally, quantitative implications of the higher-level multi-modal eco-routing framework to trip planning and city-wide energy reduction would be another worthwhile endeavor as a follow-up effort.

Appendix A

RailSIM Model Parameters

Table 10. Parameters of Dynamics and Energy Consumption Models

Name	Description	Unit
A	Acceleration	m/s^2
F_t	Tractive force	N
F_s	Starting tractive force required to move a train from a complete stop	N
R	Resistance force	N
η	Mechanical efficiency	-
λ	Throttle level	-
P_{max}	Maximum traction power	kW
u	Running speed	mi/h
μ	Coefficient of friction between the wheel and the track	-
m	Weight per railcar	ton
m_{ta} g	The railcar weight acting on the tractive axles Gravitational acceleration	kg m/s2
w_p	Weight per railcar axle	ton
K	Drag coefficient	-
n_p	Number of axles per railcar	-
θ	Track grade	%
M	Moving train weight	ton
u_d	Segment target speed	mi/h
u_m	The speed at the maximum throttle	mi/h
α_m	Ratio of running speed to desired speed at the maximum throttle	-
t_1, t_2, t_3	Throttle model parameters	-
λ∗	The minimum throttle to maintain free driving	-
F_b	Brake force	N
ω_b	Braking ratio	-
e	Efficiency of the brake lever system	-
f	Coefficient of friction between the wheel and the brake shoe	-
u_1, u_2, α, β	Brake model parameters	-
EC	Energy consumption	kW
EC_{re}	Regenerated energy power	kW
P	Tractive power	kW
HEP	Head-end power	kW
η_{re}	Regenerative efficiency	-
γ	Parameter of the regenerative efficiency model	-

References

[1] DESA, Department of Economic and Social Affairs, "*World urbanization prospects, the 2011 revision*," 2014.

[2] D. Schrank, B. Eisele, T. Lomax, and J. Bak, "*2015 urban mobility scorecard*," 2015.

[3] S. Ram, F. Dong, F. Currim, Y. Wang, E. Dantas, and L. A. Sabóia, "Smartbike: Policy making and decision support for bike share systems," in *Smart Cities Conference (ISC2), 2016 IEEE International*, 2016, pp. 1-6: IEEE.

[4] H. Rakha, M. V. Aerde, and L. Assoc., Blacksburg, VA USA, Tech. Rep, "INTEGRATION Release 2.40 for Windows: User's Guide, Volume I: Fundamental Model Features," 2013.

[5] M. Fellendorf, "VISSIM: A microscopic simulation tool to evaluate actuated signal control including bus priority," in *64th Institute of Transportation Engineers Annual Meeting*, 1994, vol. 32: Springer.

[6] M. Behrisch, L. Bieker, J. Erdmann, and D. Krajzewicz, "SUMO–simulation of urban mobility: an overview," in *Proceedings of SIMUL 2011, The Third International Conference on Advances in System Simulation*, 2011: ThinkMind.

[7] T. George Oketch, "New modeling approach for mixed-traffic streams with nonmotorized vehicles," *Transportation Research Record: Journal of the Transportation Research Board*, vol. 1705, no. 1, pp. 61-69, 2000.

[8] H. Twaddle, T. Schendzielorz, and O. Fakler, "Bicycles in urban areas: Review of existing methods for modeling behavior," *Transportation Research Record: Journal of the Transportation Research Board*, vol. 2434, no. 1, pp. 140-146, 2014.

[9] X. Ma and D. Luo, "Modeling cyclist acceleration process for bicycle traffic simulation using naturalistic data," *Transportation Research Part F: Traffic Psychology and Behaviour*, vol. 40, pp. 130-144, 2016.

[10] R. Akçelik and D. C. Biggs, "Acceleration profile models for vehicles in road traffic," *Transportation Science*, vol. 21, no. 1, pp. 36-54, 1987.

[11] K. Fadhloun, H. Rakha, A. Loulizi and A. Abdelkefi, "A Vehicle Dynamics Model for Estimating Typical Vehicle Accelerations," *Transportation Research Record: Journal of the Transportation Research Board*, vol. 35, no. 36, p. 37, 2015.

[12] A. Jahangiri and H. A. Rakha, "Applying machine learning techniques to transportation mode recognition using mobile phone sensor data," *IEEE Transactions on Intelligent Transportation Systems*, vol. 16, no. 5, pp. 2406-2417, 2015.

[13] J. C. Martin, D. L. Milliken, J. E. Cobb, K. L. McFadden, and A. R. Coggan, "Validation of a mathematical model for road cycling power," *Journal of applied biomechanics*, vol. 14, no. 3, pp. 276-291, 1998.

[14] T. Dahmen, R. Byshko, D. Saupe, M. Röder, and S. Mantler, "Validation of a model and a simulator for road cycling on real tracks," *Sports Engineering*, vol. 14, no. 2-4, pp. 95-110, 2011.

[15] D. C. POOLE, S. A. WARD, G. W. GARDNER, and B. J. WHIPP, "Metabolic and respiratory profile of the upper limit for prolonged exercise in man," *Ergonomics*, vol. 31, no. 9, pp. 1265-1279, 1988.

[16] C. G. Smith and A. M. Jones, "The relationship between critical velocity, maximal lactate steady-state velocity and lactate turnpoint velocity in runners," *European Journal of Applied Physiology*, vol. 85, no. 1-2, pp. 19-26, 2001.

[17] K. Wakayoshi *et al.*, "Does critical swimming velocity represent exercise intensity at maximal lactate steady state?," *European Journal of Applied Physiology and Occupational Physiology*, vol. 66, no. 1, pp. 90-95, 1993.
[18] J. S. Carson and O. M. Atala, "Using computer simulation for rapid transit operating strategies," in *1990 Winter Simulation Conference Proceedings*, 1990, pp. 798-801: IEEE.
[19] M. Paolucci and R. Pesenti, "An object-oriented approach to discrete-event simulation applied to underground railway systems," *Simulation*, vol. 72, no. 6, pp. 372-383, 1999.
[20] A. E. Rizzoli, N. Fornara, and L. M. Gambardella,"A simulation tool for combined rail/road transport in intermodal terminals," *Mathematics and Computers in Simulation*, vol. 59, no. 1-3, pp. 57-71, 2002.
[21] J. L. Espinosa-Aranda and R. García-Ródenas, "A discrete event-based simulation model for real-time traffic management in railways," *Journal of Intelligent Transportation Systems*, vol. 16, no. 2, pp. 94-107, 2012.
[22] X. Xiao-Ming, L. Ke-Ping, and Y. Lixing, "Discrete event model-based simulation for train movement on a single-line railway," *Chinese Physics B*, vol. 23, no. 8, p. 080205, 2014.
[23] P. Grube, F. Núñez, A. Cipriano,"An event-driven simulator for multi-line metro systems and its application to Santiago de Chile metropolitan rail network," *Simulation Modelling Practice and Theory*, vol. 19, no. 1, pp. 393-405, 2011.
[24] A. Nash and D. Huerlimann, "Railroad simulation using OpenTrack," *WIT Transactions on The Built Environment*, vol. 74, 2004.
[25] M. Asuka and K. Komaya, "A simulation method for rail traffic using microscopic and macroscopic models," *Transactions on the Built Environment*, vol. 21, 1970.
[26] M. Baohua, J. Wenzheng, C. Shaokuan, and L. Jianfeng, "A computer-aided multi-train simulator for rail traffic," in *2007 IEEE International Conference on Vehicular Electronics and Safety*, 2007, pp. 1-5: IEEE.
[27] H. N. Koutsopoulos and Z. Wang, "Simulation of urban rail operations: Application framework," *Transportation Research Record: Journal of the Transportation Research Board*, vol. 2006, no. 1, pp. 84-91, 2007.
[28] D. R. Andersen *et al.*, "Train energy and dynamics simulator (TEDS): a state-of-the-art longitudinal train dynamics simulator," in *ASME 2012 Rail Transportation Division Fall Technical Conference*, 2012, pp. 57-63: American Society of Mechanical Engineers.
[29] Q. Wu, S. Luo, and C. Cole, "Longitudinal dynamics and energy analysis for heavy haul trains," *Journal of Modern Transportation*, vol. 22, no. 3, pp. 127-136, 2014.
[30] C. Colin, "Longitudinal Train Dynamics, *Handbook of Railway Vehicle Dynamics, S. Iwnicki," ed: Boca Ratón, Taylor & Francis*, 2006.
[31] L. Cantone, "TrainDy: the new Union Internationale des Chemins de Fer software for freight train interoperability," *Proceedings of the Institution of Mechanical Engineers, Part F: Journal of Rail and Rapid Transit*, vol. 225, no. 1, pp. 57-70, 2011.
[32] J. Wang and H. A. Rakha, "Longitudinal train dynamics model for a rail transit simulation system," *Transportation Research Part C: Emerging Technologies*, vol. 86, pp. 111-123, 2018.
[33] H. Rakha, I. Lucic, S. H. Demarchi, J. R. Setti, and M. Van Aerde, "Vehicle dynamics model for predicting maximum truck acceleration levels," *Journal of Transportation Engineering*, vol. 127, no. 5, pp. 418-425, 2001.

[34] H. Rakha, M. Snare, and F. Dion, "Vehicle dynamics model for estimating maximum light duty vehicle acceleration levels," *Transportation Research Record: Journal of the Transportation Research Board*, vol. 1883, no. 1, pp. 40-49, 2004.
[35] J. Searle, "Equations for speed, time and distance for vehicles under maximum acceleration," *SAE Technical Paper 0148-7191*, 1999.
[36] W. W. Hay, *Railroad engineering*. John Wiley & Sons, 1982.
[37] J. Wang and H. A. Rakha, "Electric train energy consumption modeling," *Applied Energy*, vol. 193, pp. 346-355, 2017.
[38] C. Cole, "Longitudinal train dynamics," Handbook of Railway Vehicle Dynamics, *CRC Press, Taylor & Francis Group*, pp. 239-277, 2006.
[39] J. Wang and H. A. Rakha, "Fuel consumption model for conventional diesel buses," *Applied Energy*, vol. 170, pp. 394-402, 2016.
[40] J. Wang and H. A. Rakha, "Convex fuel consumption model for diesel and hybrid buses," *Transportation Research Record: Journal of the Transportation Research Board*, vol. 2647, no. 1, pp. 50-60, 2017.
[41] F. E. Gbologah, Y. Xu, M. O. Rodgers, and R. Guensler, "Demonstrating a bottom-up framework for evaluating energy and emissions performance of electric rail transit options," *Transportation Research Record: Journal of the Transportation Research Board*, vol. 2428, no. 1, pp. 10-17, 2014.
[42] J. Powell and R. Palacín, "Passenger stability within moving railway vehicles: limits on maximum longitudinal acceleration," *Urban Rail Transit*, vol. 1, no. 2, pp. 95-103, 2015.